DNA Repair 113 (2022) 103320

Contents lists available at ScienceDirect

DNA Repair

journal homepage: www.elsevier.com/locate/dnarepair

Expression of BRCA1, BRCA2, RAD51, and other DSB repair factors is regulated by CRL4^{WDR70}

Zachary Mirman [a,1], Keshav Sharma [a], Thomas S. Carroll [b], Titia de Lange [a,*]

[a] Laboratory for Cell Biology and Genetics, The Rockefeller University, New York, NY 10065, USA
[b] Bioinformatics Resource Center, The Rockefeller University, New York, NY 10065, USA

ARTICLE INFO

Keywords:
WDR70
DSB repair
Homology-directed repair
5′ End resection
53BP1
BRCA1
RAD51
CRL4/DDB1

ABSTRACT

Double-strand break (DSB) repair relies on DNA damage response (DDR) factors including BRCA1, BRCA2, and RAD51, which promote homology-directed repair (HDR); 53BP1, which affects single-stranded DNA formation; and proteins that mediate end-joining. Here we show that the CRL4/DDB1/WDR70 complex (CRL4^{WDR70}) controls the expression of DDR factors. Auxin-mediated degradation of WDR70 led to reduced expression of BRCA1, BRCA2, RAD51, and other HDR factors; 53BP1 and its downstream effectors; and other DDR factors. In contrast, cNHEJ factors were generally unaffected. WDR70 loss abrogated the localization of HDR factors to DSBs and elicited hallmarks of genomic instability, although 53BP1/RIF1 foci still formed. Mutation of the DDB1-binding WD40 motif, disruption of DDB1, or inhibition of cullins phenocopied WDR70 loss, consistent with CRL4, DDB1, and WDR70 functioning as a complex. RNA-sequencing revealed that WDR70 degradation affects the mRNA levels of DDR and many other factors. The data indicate that CRL4^{WDR70} is critical for expression of myriad genes including BRCA1, BRCA2, and RAD51.

1. Introduction

Genome integrity is maintained in part by a tightly regulated DNA damage response (DDR) [1]. Repair pathways for ssDNA damage, DSBs, and replication-associated damage involve a large network of well-studied factors, although many remain poorly understood at a mechanistic level. High-fidelity DSB repair can be mediated by classical non-homologous end-joining (cNHEJ) or homology-directed repair (HDR). cNHEJ, mediated by KU70/80, DNA-PKcs, LIG4, XRCC4, and accessory factors, ligates minimally-processed DNA ends throughout the cell cycle. HDR requires 5′ end resection and a homologous template, conditions that are met after DNA replication in S/G2 [2]. HDR is dependent on the tumor suppressors BRCA1 and BRCA2 acting with RAD51 and a host of other factors [3,4]. BRCA1 is thought to promote overhang formation, and also plays a role with BRCA2 in the loading of RAD51 on ssDNA [5]. The requirement for BRCA1 in HDR can be bypassed by loss of 53BP1, which results in formation of ssDNA at DSBs. As a result, the sensitivity BRCA1-deficient cells to PARP inhibitors (PARPi) [6] is diminished when 53BP1 or its downstream effectors (RIF1, shieldin, and CST/Polα/primase) are removed [7–20]. Because 53BP1 promotes the misrejoining of DSBs in PARPi-treated BRCA1-deficient cells, 53BP1 has been proposed to govern the choice between cNHEJ and HDR [21]. An alternative view is that the attributes of 53BP1 evolved to ensure DSB repair fidelity [22].

In addition to HDR, DSBs that have undergone resection can be acted on by PARP1-, LIG3-, and POLQ-dependent alternative non-homologous end-joining (aNHEJ). This pathway is error-prone due to its reliance on microhomologies exposed by resection [23] and is repressed in most settings. A second error-prone DSB repair pathway is single-strand annealing (SSA), which is mediated by RAD52 [24].

WDR70 is thought to function as part of the DDB1-Cullin Ring Ligase 4 (CRL4) complex [25]. CRL complexes are modular ubiquitin ligases with diverse roles in mammalian cell biology, including in DNA repair [26,27]. They are composed of a scaffold (cullin family protein), a RING finger protein (e.g., Rbx1), a linker protein (e.g. DDB1), and one of many substrate specificity factors (e.g. WDR70) [26]. Recent data suggests that CRL4^{WDR70} plays a role in the DDR. In fission yeast, WDR70 promotes resection through histone H2B mono-ubiquitination by opposing Crb2^{53BP1} [25]. Yeast WDR70 plays multiple roles in cell cycle progression, chromatin structure, and DNA repair by HDR [28]. Human

* Corresponding author.
E-mail address: delange@rockefeller.edu (T. de Lange).
[1] Current address: Division of Genetics, Brigham and Women's Hospital, Howard Hughes Medical Institute, Department of Genetics, Harvard Medical School, Boston, MA 02115, USA.

https://doi.org/10.1016/j.dnarep.2022.103320
Received 28 December 2021; Received in revised form 7 March 2022; Accepted 11 March 2022
Available online 15 March 2022

WDR70 has also been linked to resection and HDR [25,29]. Intriguingly, DDB1 was identified in an siRNA screen for genes whose loss—like BRCA1/2—sensitizes cells to PARPi [30], hinting at a role in HDR.

Because WDR70 appears to be essential in human cells (https://depmap.org/portal) and other organisms [31], we created RPE1 cells in which the endogenous WDR70 can be degraded with an auxin-inducible degron (AID) [32]. Using this system, we confirm that WDR70 is essential for cell viability and report that acute loss of WDR70 triggers genome instability. This phenotype is accompanied by a significant reduction in the expression levels of BRCA1, BRCA2, RAD51, and other proteins involved in HDR and abrogation of DSB-induced focus formation by these factors. WDR70 loss also reduces the expression of 53BP1 and its downstream factors as well as proteins involved in aNHEJ and SSA. In contrast, factors involved in cNHEJ and apical DDR factors, such as the ATM kinase and RNF8, were unaffected. Based on mutations in WDR70, depletion of DDB1, and chemical inhibition of cullin activity, we conclude that WDR70 acts as part of a complex with CRL4/DDB1. In agreement with the reduction in protein levels of HDR factors, RNA sequencing in WDR70-depleted cells showed a dramatic reduction in the transcripts of BRCA1, BRCA2, RAD51, and other HDR genes, along with substantial additional transcriptomic changes. These data reveal a novel shared regulation of proteins involved in specific DSB repair pathways by the $CRL4^{WDR70}$ complex.

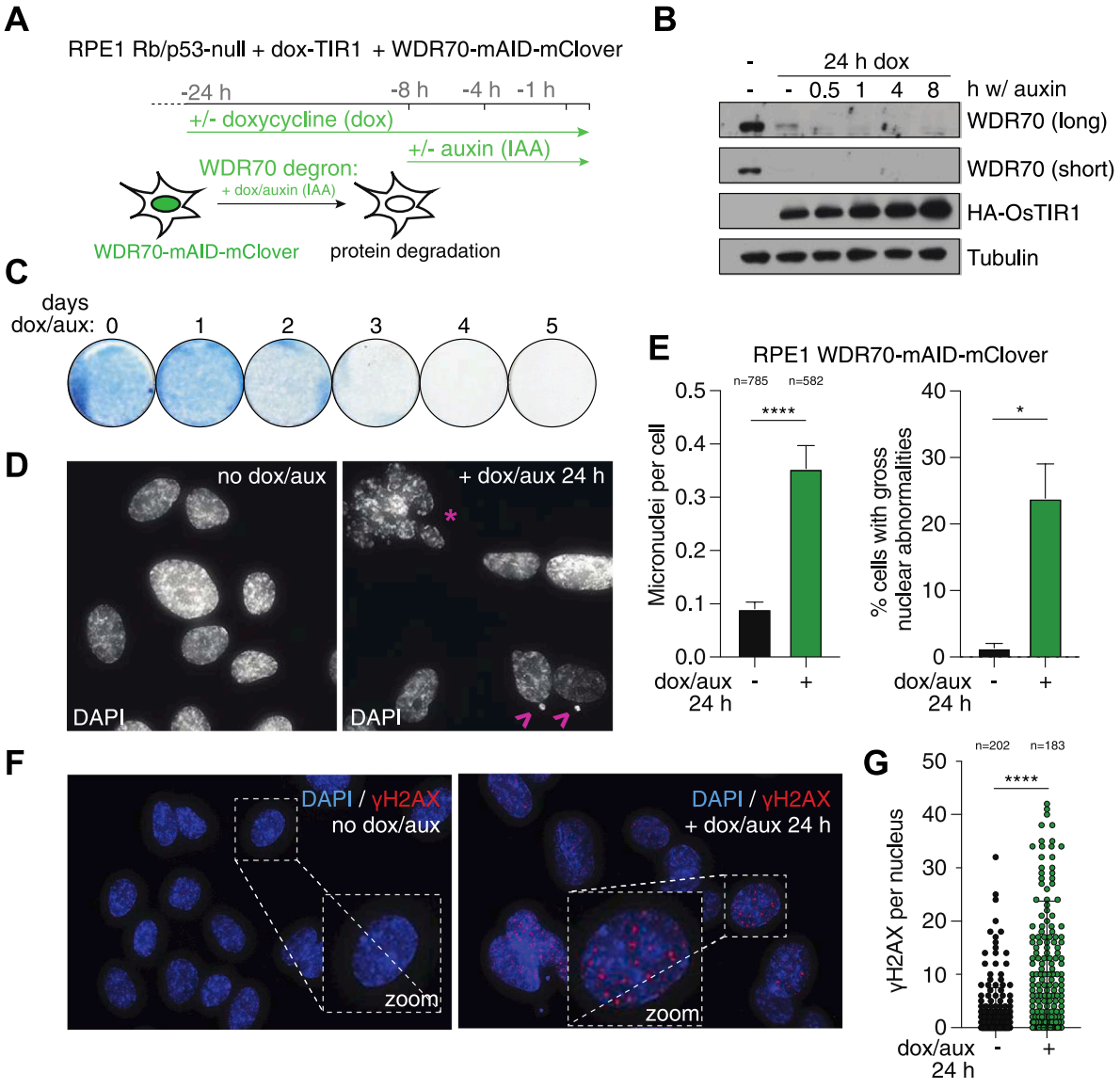

Fig. 1. WDR70 is essential for genome integrity. **(A)** Experimental timeline and schematic representation of auxin-induced degradation of WDR70 in RPE1 cells. HA-tagged OsTIR1 expression is doxycycline (dox)-inducible, and addition of indole-3-acetic acid (IAA, auxin) triggers WDR70 degradation. **(B)** Immunoblot for the indicated proteins in cells as in **(A)** showing dox/auxin-mediated degradation of WDR70. The full blot also appears in Fig. S1D, where an independent clone showed the same effect. **(C)** Survival assay for cells in which WDR70 is degraded. Cells in 6-well plates were treated with dox/auxin for the indicated number of days and then harvested by methylene blue staining. **(D)** Representative images of DAPI-stained nuclei in control cells or cells treated with dox/auxin for 24 h. Micronuclei (MN) are indicated by the arrowheads, and a gross nuclear abnormality is indicated by the asterisk. **(E)** Quantification of cells as in **(D)** for micronuclei per cell (the number of cells per condition (n) pooled from three independent experiments is shown) and gross nuclear abnormalities from three independent experiments. **(F)** Representative images of control cells or cells treated with dox/auxin for 24 h monitored for γH2AX foci formation. **(G)** Quantification of cells as in **(F)**. The number of nuclei (n) pooled from three independent experiments is shown. For all panels, data is from three independent experiments. Statistical analysis based on two-tailed Welch's t-test. * , $p < 0.05$; ** , $p < 0.01$; *** , $p < 0.001$; **** , $p < 0.0001$; ns, not significant.(For interpretation of the references to colour in this figure, the reader is referred to the web version of this article.)

2. Results

2.1. WDR70 is essential for genome integrity

To examine the phenotype of WDR70 loss, we generated cells in which endogenous WDR70 can be degraded rapidly using the AID/TIR1 system [32] (Fig. S1A). CRISPR/Cas9 was used to achieve biallelic knock-in of mini AID (mAID) fused to mClover into the *WDR70* loci of p53/RB-null RPE1 cells [33]. Biallelic targeting was confirmed by western blot (Fig. S1B). Subclones harboring lentiviral dox-inducible HA-tagged OsTIR1 were generated (Fig. S1C) such that doxycycline (dox) and auxin (aux) addition in two independent clones resulted in rapid loss of WDR70 protein (Fig. S1D). We used one of these clones, hereafter referred to as WDR70-degron cells, to examine the effects of WDR70 loss in RPE1 cells. WDR70 protein was reduced by dox treatment and became undetectable 0.5 h after addition of auxin to dox-treated cells (Fig. 1A, B). WDR70-depleted cells experienced impaired cell cycle progression and reduced BrdU incorporation as

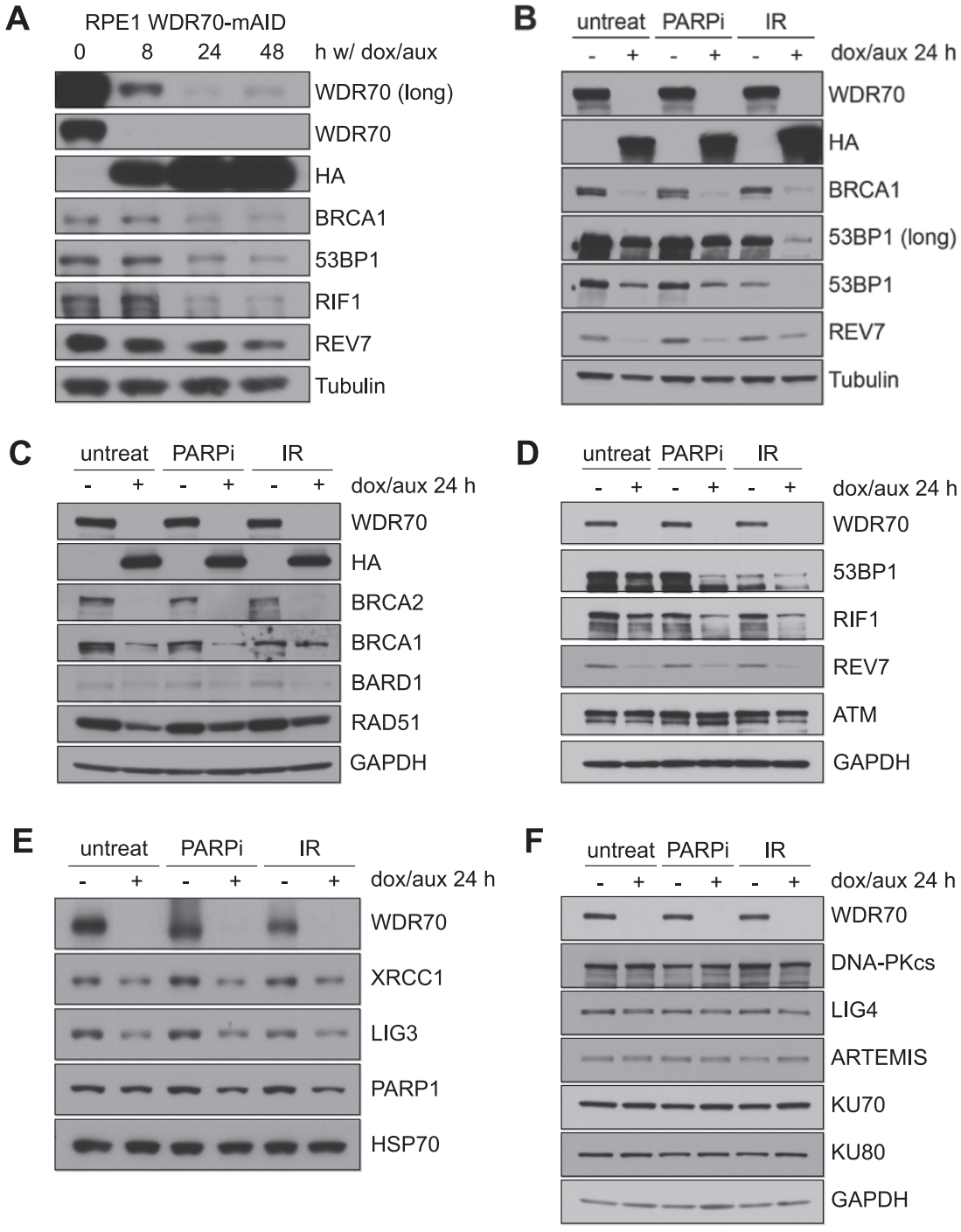

Fig. 2. WDR70 regulates DNA damage response factors. **(A)** Immunoblot for the indicated proteins in WDR70-degron cells after dox/auxin treatment. **(B)** Immunoblot analysis in cells as in **(A)** treated with Olaparib (2 μM, 24 h) or IR (5 h after 5 Gy), with or without dox/auxin for 24 h. **(C–F),** Immunoblot analysis of **(C)** HDR factors, **(D)** 53BP1 pathway factors, **(E)** aNHEJ factors, and **(F)** cNHEJ factors in cells treated as in **(B)**. All blots are representative of three independent experiments. Because of the dramatic effect of WDR70 loss on DDR pathway components, protein concentrations were checked by BCA assay and Ponceau stains to ensure equal loading, and three distinct loading controls were employed (γTubulin, GAPDH, and HSP70), all of which were unchanged by WDR70 loss.

judged by flow cytometry (Fig. S1E, F), and ultimately death with prolonged dox/auxin treatment (Fig. 1C). Furthermore, DAPI-stained nuclei showed increased frequency of micronucleation, gross nuclear abnormalities, and elevated levels of γH2AX foci, all hallmarks of genomic instability (Fig. 1D-G). These data indicate that WDR70 is required for normal cell cycle progression and genome integrity.

2.2. WDR70 regulates DNA damage response factors

Immunoblotting showed that degradation of WDR70 resulted in loss of BRCA1, BRCA2, BARD1, and RAD51 (Fig. 2A–C). Loss of these HDR factors in WDR70-depleted cells was accompanied by loss of the BRCA-associated and HDR-relevant factors ABRAXAS, RAP80, PALB2, the nuclease EXO1, and the RecQ helicase WRN [3] (Fig. S2A). The loss of these factors was not apparent after 8 h dox/aux treatment when some WDR70 remained but became obvious at 24 h when WDR70 was no longer detectable (Fig. 2A). We therefore continued with the longer treatment protocol in subsequent experiments. The effect of WDR70 loss was independent of DNA damage and not further exacerbated by treatment with PARPi (Olaparib) or ionizing radiation (IR) (Fig. 2B, C). WDR70 protein levels were similar in asynchronous cells and in cells arrested in G2 by RO-3306, and BRCA1 loss was observed in G2 (Fig. S2B). Therefore, the effect of WDR70 degradation is not affected by DNA damage and is consistent between asynchronous or G2-enriched cells.

In addition to the HDR factors, 53BP1 and its downstream effectors RIF1 and REV7 were strongly diminished after WDR70 degradation (Fig. 2A-D). REV7 is a subunit of the shieldin complex along with SHLD1, SHLD2, and SHLD3 [34]. SHLD2 expression was reduced after WDR70 degradation (Fig. S2C). Reduced expression was also observed for two subunits of the CST complex, CTC1 and STN1, as well as Polα and primase, which act downstream of 53BP1-shieldin to mediate fill-in synthesis at DSBs [17,58] (Fig. S2D, E). Some factors involved in aNHEJ (XRCC1 and Ligase 3) were also regulated by WDR70 while others (PARP1) were not (Fig. 2E). RAD52, which promotes single-strand annealing was also decreased in WDR70-depleted cells (Fig. S2F).

A number of proteins relevant to DSB repair were not affected by WDR70 degradation. ASTE1, a structure-specific endonuclease that localizes to DSBs downstream of shieldin and promotes NHEJ [35], was unaffected by WDR70 loss (Fig. S2D) as were factors acting upstream of 53BP1 in the DDR signaling cascade (ATM, RNF8) (Fig. 2D, Fig. S2G). None of the cNHEJ factors querried (KU70/80, DNA-PKcs, Artemis, LIG4) were affected by WDR70 loss (Fig. 2F) and neither were the

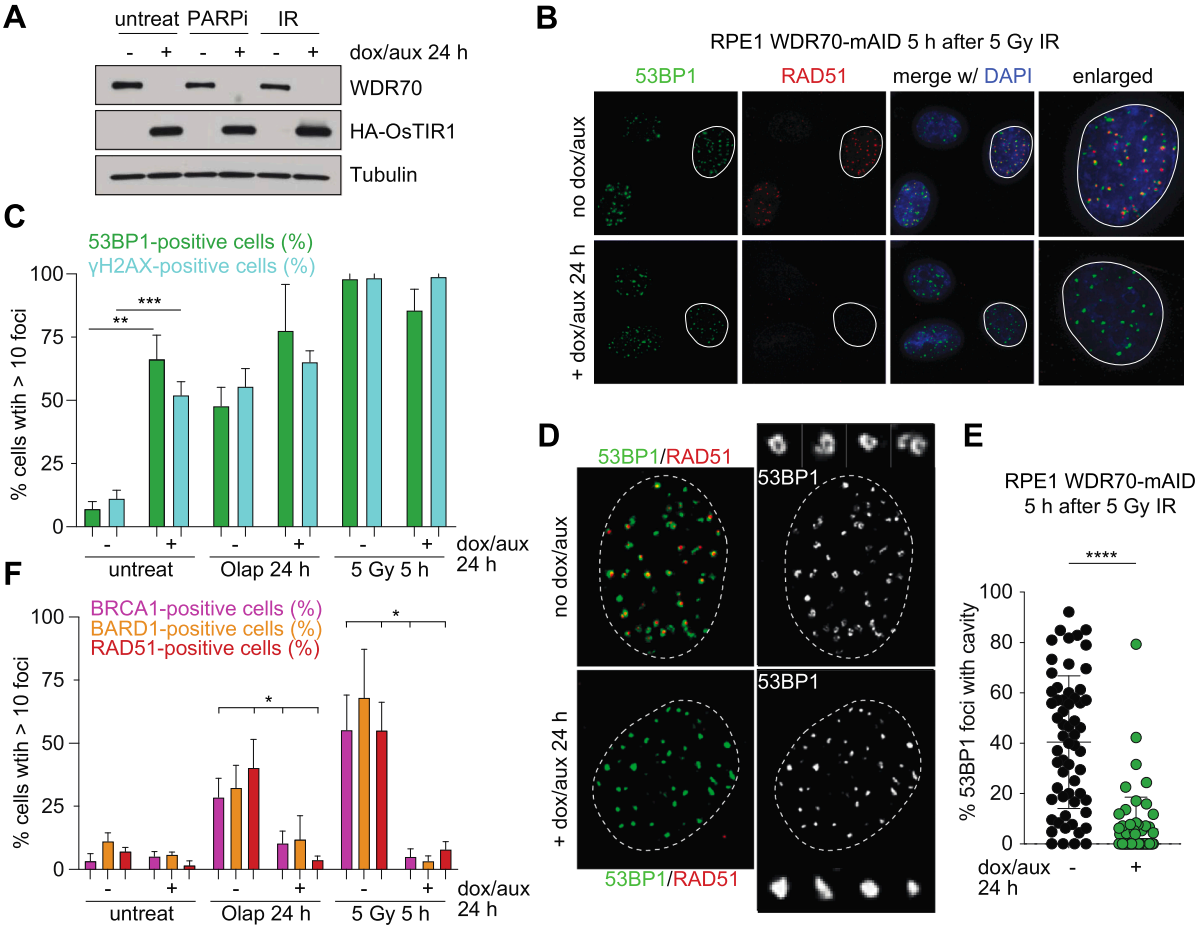

Fig. 3. The effect of WDR70 loss on DNA damage foci. **(A)** Immunoblots for WDR70 and HA-OsTIR1 in WDR70-degron cells untreated or treated with Olaparib (2 μM, 24 h) or IR (5 h after 5 Gy), with or without dox/auxin for 24 h. **(B)** Representative IF images of 53BP1 (green) and RAD51 (red) co-stain in irradiated cells as in **(A)**. Dashed lines demarcate nuclear outline; one sample cell is enlarged at right. **(C)** Quantification of percent of cells with greater than 10 foci in cells as in **(A)**. Bar graph depicts mean and sd from three independent experiments. **(D)** Representative images depicting 53BP1 and RAD51 foci architecture in the indicated irradiated cells. Right panel (53BP1) includes four enlarged foci from each nucleus. **(E)** Quantification of the percent of 53BP1 foci with a cavity (see Materials and methods for scoring rubric) in irradiated cells as in **(D)**. Data pooled from three independent experiments. 60 nuclei (each represented by a dot) were scored per condition. **(F)** Quantification of percent of cells with greater than 10 foci as in **(C)**. Bar graph depicts mean and sd from two (BARD1) or three (BRCA1, RAD51) independent experiments. All statistical analyses as in Fig. 1.(For interpretation of the references to colour in this figure, the reader is referred to the web version of this article.)

cohesin complex and PCNA (Fig. S2H). Collectively, the data reveal that WDR70 regulates the expression of DSB repair proteins in a manner that is selective to certain pathways. Specifically, the DDR proteins that are affected by WDR70 create, regulate, or rely on DSB resection.

2.3. The effect of WDR70 loss on DNA damage foci

To determine whether WDR70 loss affects the ability of DDR factors to form DNA damage foci, we performed immunofluorescence (IF) after induction of DNA damage with PARPi or IR (Fig. 3A-C). As shown above (Fig. 1F, G), WDR70 loss itself induced a modest level of γH2AX foci, even in the absence of DNA damage (Fig. 3C). After PARPi- or IR-treatment of WDR70-depleted cells, the same level of γH2AX foci occurred as in WDR70-proficient cells, confirming that ATM and/or ATR signaling remained intact (Fig. 3C).

We suspected that the ability of factors whose protein levels were

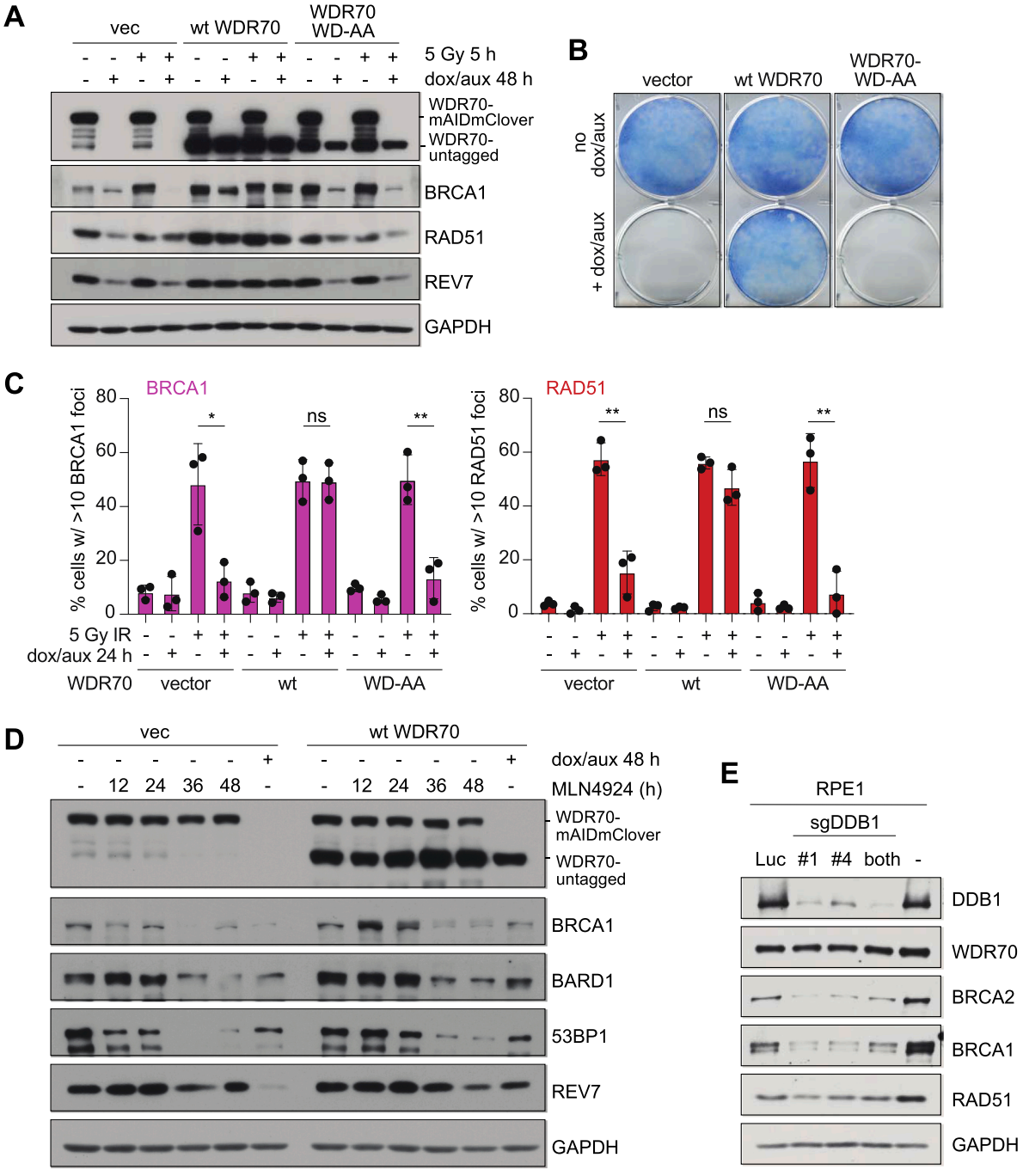

Fig. 4. WDR70 functions via its DWD motif as part of a CRL4 complex. **(A)** Immunoblots for the indicated proteins in WDR70-degron cells complemented with empty vector (vec) or the indicated WDR70 constructs. Cells were treated with IR (5 h after 5 Gy) and/or dox/auxin for 48 h as indicated. In the top blot, WDR70 antibody detects the knock-in mAID-mClover-tagged WDR70 and the exogenously expressed untagged WDR70 wild-type or WD-AA mutant. **(B)** Cell survival assay for RPE1 WDR70-degron cells complemented with empty vector or the indicated WDR70 constructs. Experimental schematic in Fig. S4B. **(C)** Quantification of percent of cells with greater than 10 foci in WDR70-degron cells with the indicated treatments. Bar graph depicts mean and sd from three independent experiments. **(D)** Immunoblots for the indicated proteins in WDR70-degron cells complemented with empty vector or wild-type WDR70. Cells were treated with the pan-cullin inhibitor MLN4924 for the indicated time, or 48 hr of dox/auxin treatment. **(E)** Immunoblots for the indicated proteins in RPE1 cells treated with bulk CRISPR KO targeting *luciferase* (Luc) or *DDB1*. All panels are representative of three independent experiments. Statistical analyses as in Fig. 1.

affected by WDR70 loss would be compromised in their ability to form DNA damage foci. But interestingly, WDR70 loss did not diminish 53BP1 foci in response to DNA damage (Fig. 3B, C; Fig. S3A), despite the dramatic loss of 53BP1 protein seen in immunoblots following irradiation (Fig. 2A-D). However, the architecture of the 53BP1 foci was altered. 53BP1 forms ring- or horseshoe-shaped microdomains that encircle BRCA1, RAD51, and RPA and this distinctive architecture is dependent on BRCA1 [36,37]. Consistent with their reduced BRCA1 expression, WDR70-depleted cells had 53BP1 foci that did not show the horseshoe shape and were more globular (Fig. 3D, E). RIF1 also retained its ability to form IR-induced foci even in the absence of WDR70 (Fig. S3B).

We next examined the ability of HDR factors to form DNA damage foci. In contrast to γH2AX and 53BP1/RIF1, the ability of BRCA1, BARD1, and RAD51 to form DNA damage foci was abrogated by WDR70 loss (Fig. 3B, F; Fig. S3C-E). WDR70-depleted cells that did not experience PARPi or IR also showed a reduction in RAD51 foci, suggesting that

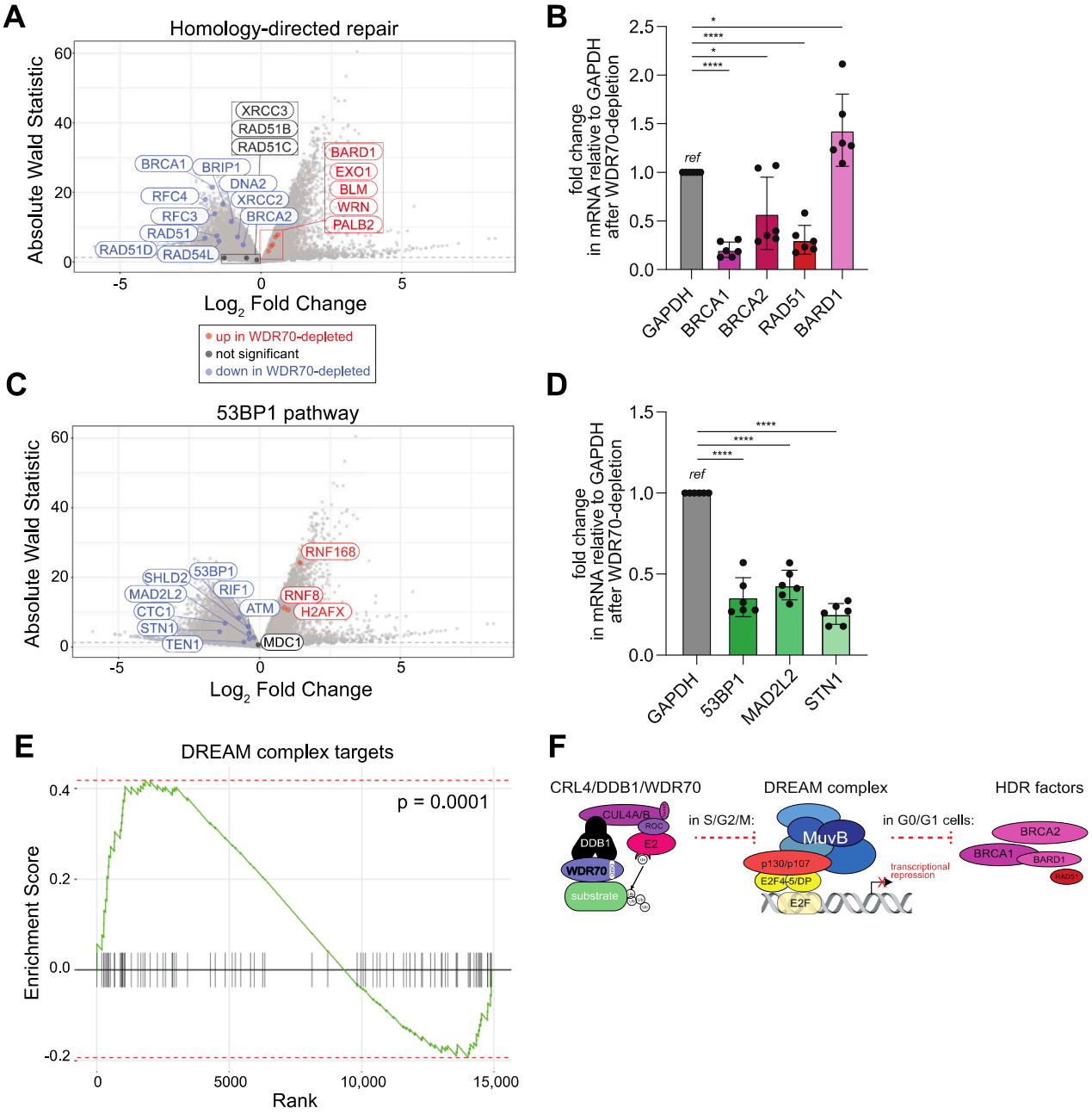

Fig. 5. WDR70 loss affects RNA levels of DDR and other factors. **(A)** Volcano plot depicting Log_2 fold change and absolute Wald Statistic for transcripts in WDR70-depleted cells (dox and aux for 24 h). Negative Log_2 fold change (blue dots and labels) indicates transcripts which are less abundant in WDR70-depleted cells. Positive Log_2 fold change (red dots and labels) indicates transcripts which are more abundant in WDR70-depleted cells. Absolute Wald Statistic above 1.96 (marked by the dashed line) is considered significant. Black dots and labels indicate genes which were not differentially regulated. Transcripts of factors involved in HDR are highlighted. **(B)** RT-PCR data showing the fold change in mRNA of the indicated HDR genes relative to GAPDH in WDR70-depleted cells. Two primer pairs were used for each gene in three independent biological replicates. **(C)** As in (A), except transcripts of genes involved upstream and downstream of 53BP1-mediated DSB processing are highlighted. **(D)** As in (B), except for 53BP1 pathway genes. **(E)** GSEA plot showing differential expression in WDR70-depleted cells of 88 predicted targets of the DREAM complex. Genes are ranked along the x-axis with the most downregulated genes in WDR70-depleted cells at the left. **(F)** Speculative model for how $CRL4^{WDR70}$ and DREAM control the expression of HDR factors BRCA1, BRCA2, and RAD51 among others.(For interpretation of the references to colour in this figure, the reader is referred to the web version of this article.)

the defect in RAD51 loading extends to endogenous DNA damage as well as PARPi or IR treatment (Fig. S3E). As expected, the loss of BRCA1 and RAD51 foci correlated with the change in 53BP1 architecture noted above (Fig. 3D, E). These results demonstrate that WDR70 specifically promotes the ability of HDR factors to coalesce into DSB foci.

2.4. WDR70 functions via its DWD motif as part of a CRL4/DDB1 complex

To determine whether the effects of WDR70 degradation were due to loss of its role in the CRL4/DDB1 complex, we tested whether mutation of the DDB1-interacting WD motif (DWD) of WDR70 [38] affected its function. The wild-type (wt) WDR70 was expressed slightly higher than the endogenous mAID-tagged WDR70, while the WD-AA mutant of WDR70 was expressed at similar levels to the endogenous WDR70 (Fig. 4A). Importantly, the loss of BRCA1 and RAD51 in WDR70-depleted cells was mitigated by wt WDR70 but not the WD-AA mutant (Fig. 4A), indicating a functional role for these residues. The REV7 component of shieldin showed the same trend (Fig. 4A). The WDR70-dependent effects on protein stability were observed at 24 h of dox/auxin treatment (Fig. S4A) but were more pronounced at 48 h (Fig. 4A). The cell death elicited by WDR70 loss was reversed by wt WDR70 but not the WD-AA mutant (Fig. S4B; Fig. 4B). Additionally, the failure of WDR70-depleted cells to form BRCA1 and RAD51 foci was fully complemented by wt WDR70 but not the WD-AA mutant (Fig. 4C). The 53BP1 foci observed in WDR70-depleted cells without DNA damaging agents (Fig. 3C) were suppressed by wt WDR70 but not the WD-AA mutant (Fig. S4C).

Supporting a role for WDR70 as part of a complex with CRL4/DDB1, a pan-cullin inhibitor MLN4924 [39] resulted in the progressive loss of BRCA1, BARD1, 53BP1, and REV7 (Fig. 4D; Fig. S4D). Overexpression of wt WDR70 did not reverse the effect of MLN4924, although it again rescued the protein loss phenotypes associated with WDR70 degradation (Fig. 4D). We also used bulk CRISPR KO with two sgRNAs to disrupt the CUL4 linker DDB1 [26,30,38]. DDB1 KO with both sgRNAs together or individually reduced the levels of BRCA2, BRCA1, and RAD51 (Fig. 4E) in a manner that is reminiscent of the effect of WDR70 loss (Fig. 2), although WDR70 levels were not affected by targeting DDB1 (Fig. 4E). Taken together, these results suggest that the expression of DDR factors promoted by WDR70 occurs in the context of a $CRL4^{WDR70}$ complex.

2.5. WDR70 loss affects transcript levels of HDR and other DDR factors

We performed bulk RNA sequencing in WDR70-degron cells to test whether the loss of DDR proteins was due to a decrease in the mRNA levels of the corresponding genes. Total RNA was extracted from WDR70-depleted cells for comparison to control cells. Many factors were differentially regulated between cells with and without WDR70 (Fig. 5A), but reassuringly, BRCA1 and RAD51 emerged as two of the most significantly down-regulated genes in WDR70-depleted cells (Fig. 5A). Transcripts of the HDR factors BRCA2, BRIP1 (or BACH1/FANCJ), RAD51D, RAD54L, and others were also significantly diminished in WDR70-depleted cells (Fig. 5A). PALB2, EXO1, and WRN, which were decreased in WDR70-depleted cells at the protein level (Fig. S2A) were slightly elevated by RNAseq (Fig. 5A). We confirmed the decrease seen in BRCA1, BRCA2, and RAD51 mRNA seen by RNAseq using RT-PCR (Fig. 5B; Fig S5A). These results are in agreement with the decrease in protein levels (Fig. 2; Fig S5B). BARD1 showed mildly increased mRNA levels in WDR70-depleted cells (Fig. 5A, B; Fig. S5A), though BARD1 protein was slightly decreased in cells lacking WDR70 (Fig. 2C), perhaps because of the more dramatic loss of its obligate binding partner, BRCA1 (Fig. 5A; Fig. 2C).

RNA sequencing of WDR70-depleted cells also revealed a decrease in transcripts of 53BP1, RIF1, MAD2L2 (REV7), SHLD2, and the CST complex (Fig. 5C), in agreement with the loss of these proteins upon WDR70 degradation (Fig. 2A, B, D; Fig. S2C, D; Fig S5B). Upstream DDR signaling factors including ATM, MDC1, and γH2AX were modestly changed or unchanged, while RNF8 and RNF168 showed an increase (Fig. 5C). We validated the change in mRNA levels for 53BP1, MAD2L2, and STN1 by RT-PCR (Fig. 5D; Fig. S5A). cNHEJ factors which were unchanged at the protein level in WDR70-depleted cells were mildly affected by WDR70 loss in the RNAseq data set (LIG4, PRKDC (DNA-PK), DCLRE1C (Artemis), and NHEJ1 (XLF)) (Fig. S5C). Surprisingly, XRCC5/6 (KU70/80) transcripts were increased (Fig. S5C) despite protein levels being unaffected by WDR70 loss (Fig. 2F). In WDR70-depleted cells, transcript levels for the aNHEJ pathway genes XRCC1, LIG3, and PARP1 (Fig. S5D) corresponded to the protein levels of those factors reported above (Fig. 2E).

Many genes involved in cell cycle control, DNA replication and repair, and transcriptional regulation were affected by WDR70 loss. The collective regulation of myriad cell cycle components and particularly DDR factors was reminiscent of the DREAM complex, a p130-containing RB-like complex which usually functions as a transcriptional repressor at E2F or CHR elements but upon dissociation of p130 and E2F can also act as an activator [40,41]. Meta-analyses have suggested hundreds of targets of the DREAM complex including BRCA1, BRCA2, RAD51, and other DDR factors [42,43]. We queried our RNAseq dataset to determine whether 88 predicted DREAM targets [42] were affected by WDR70 loss. Indeed, WDR70 loss caused significant dysregulation of DREAM targets, with some strongly increased and others substantially decreased (Fig. 5E; Fig. S5E). Finally, we noted that POLR2A, the catalytic subunit of RNA polymerase II, was dramatically reduced in WDR70-depleted cells at the RNA and protein level (Fig. S5F) which may account (in part) for reduced transcription of some genes, although many were significantly increased as well (Fig. 5A, C). Collectively, the data indicate that WDR70 loss has a broad effect on cellular mRNA levels including the reduction of transcripts of many HDR and 53BP1 pathway factors, which corresponded to the loss of those factors observed at the protein level.

2.6. H2BK120R does not affect RAD51 loading or PAPRi-induced radial formation

It was previously proposed that the monoubiquitination of H2B promoted by $CRL4^{WDR70}$ impacted resection and therefore HDR [25,28]. We expressed a dominant negative histone, H2BK120R, which cannot be ubiquitinated [44], yet this did not recapitulate BRCA1 phenotypes like loss of RAD51 loading or PARPi-induced radial chromosomes (Fig. S6A, B). Loss of WDR70 also did not affect levels of RNF20, the ubiquitin ligase responsible for depositing H2BK120Ub (Fig. S6C) [44,45]. We did observe minor decreases in H2BK120ub after WDR70 loss, in agreement with past experiments [25,28,46] (Fig. S6D). These data argue against a direct role for WDR70 in promoting resection through ubiquitination of H2B.

3. Discussion

By employing the auxin system for rapid degradation of WDR70 in combination with targeted immunoblotting and bulk RNA sequencing, we identified a broad role for $CRL4^{WDR70}$ in maintaining the normal proteome and transcriptome. WDR70 affects transcript and protein levels of factors from multiple DSB repair pathways but is particularly relevant to HDR. BRCA1 and RAD51 mRNA and protein levels were reduced after WDR70 degradation, and those factors failed to form DNA damage foci. WDR70 loss had a pronounced effect not only on HDR factors, but also members of the 53BP1/RIF1/shieldin/CST/Polα/primase pathway, aNHEJ, and RAD52; in contrast, upstream factors in the DDR and those involved in cNHEJ were largely unaffected.

How does WDR70 loss lead to this striking phenotype? One candidate for such regulation is the DREAM complex [40,41]. Many cell cycle and DDR genes including BRCA1, BRCA2, and RAD51 have promoters which are bound by subunits of the DREAM complex [40,42,43]. We

observed that in WDR70-depleted cells a group of predicted DREAM targets were strongly dysregulated (Fig. 5E; Fig. S5E). The subunit composition and the activity of the DREAM complex depends on the cell cycle phase. The MuvB subunits of the DREAM complex dissociate from p130/p107 and associate with FOXM1 or B-MYB to function as a transcriptional activator in S/G2/M, while the repressive role of the DREAM complex is pronounced in G0/G1 cells [40,41,47]. We speculate that when $CRL4^{WDR70}$ is disrupted, this repressive effect of the DREAM complex—which is normally restricted to G0/G1 [47]—may extend to S/G2/M (Fig. 5F). Perhaps $CRL4^{WDR70}$ degrades an inhibitor of the DREAM complex in S/G2/M or otherwise antagonizes the DREAM complex in a cell-cycle-regulated manner. Our work hints at a connection between $CRL4^{WDR70}$ and the DREAM complex, but testing this will require further analysis across cell types and cell cycle phases.

It has also been observed that hypoxia induces loss of HDR proteins [48–50] in a manner reminiscent of WDR70-depleted cells, but it is not known how WDR70 may be affected by hypoxia. We note that hypoxia-inducible factor 1 alpha inhibitor (HIF1AN) mRNA levels were substantially lower in WDR70-depleted cells (Log2 fold change = −1.85; $p = 3.88 \times 10^{-36}$), so it is feasible that a transcriptional program like that of HIF1a stabilization is instated upon WDR70 loss. A noteworthy finding from our RNAseq of WDR70-degron cells was that POLR2A transcripts were decreased in cells lacking WDR70, suggesting that transcription may be reduced globally. However, some mRNAs (e.g., those pertaining to some upstream DDR signaling or cNHEJ factors) were unaffected, and indeed many were increased after 24 h of WDR70 degradation. The WDR70 phenotype, therefore, cannot be explained by decreased transcription alone. Whether WDR70 acts through known transcriptional regulators like the DREAM complex or HIF1a or through another mechanism, the regulation (and indeed, the selective advantage) of such a cellular program which affects many resection-relevant DDR factors will be of interest. RNA sequencing in yeast wdr70Δ cells did not reveal major transcriptional differences as compared to wild-type cells [25], suggesting that the regulatory function of WDR70 may have evolved in higher eukaryotes. Studies in yeast proposed a role for WDR70 in promoting resection through ubiquitination of H2B [25,28], but human WDR70 affects the expression of myriad genes with two of the most affected genes being BRCA1 and RAD51. Therefore, our data raise the possibility that the effect of WDR70 on resection and HDR is indirect.

BRCA1 and 53BP1, which have been discussed as determinants of DSB repair pathway choice, were decreased at the levels of mRNA and protein after WDR70 degradation (Figs. 2, 5). However, 53BP1/RIF1 foci formation was unaffected by WDR70 loss, while HDR foci formation was abrogated (Fig. 3). It is plausible that defects in WDR70 activity could resemble HDR-deficient cells or cancers, but the essential and pleiotropic nature of WDR70 [28,51] argue against the likelihood of total loss of function of the gene in cancer.

4. Materials and methods

4.1. Cell culture and expression constructs

293FT and Phoenix A cells were cultured in Dulbecco's Modified Eagle Medium (DMEM, Corning) supplemented with 10% bovine calf serum (BCS), non-essential amino acids (Gibco), 2 mM L-glutamine (Gibco), 100 U/ml penicillin, 100 μg/ml streptomycin (Gibco). RPE1 cells were cultured in DMEM/F-12 media (Gibco) supplemented with 10% fetal bovine serum (FBS) and penicillin/streptomycin as above.

Retroviral gene delivery was performed as described [52]. For pLPC-WDR70, human WDR70 cDNA (Genscript) was amplified and cloned into pLPC-Puro. pLPC-WDR70-WD-AA mutant was generated by Gibson assembly using primers containing the 404 W 405D to 404 A 405 A mutation: TGG GAC to GCG GCT.

Drug treatments were as follows. Olaparib (Selleck Chemicals): 2 μM unless otherwise noted; Doxycycline (dox, Sigma): 2 μg/ml. IAA (auxin, 3-indole-acetic acid sodium salt dissolved in H_2O, Abcam): 500 μM. MLN4924 (Sigma): 20 μM.

4.2. CRISPR-Cas9 gene editing

For the generation of RPE1 WDR70-mAID-mClover cells, p53/Rb-null RPE1 cells [33] were nucleofected with a donor template plasmid and two CRISPR/Cas9 pX330 plasmids targeting the last coding exon of *WDR70* [32]. sgRNA 1: (5′-TGAGAGCTGTTTGCATGAGT-(PAM)−3′); sgRNA 2: (5′-TTGAGAGCTGTTTGCATGAG-(PAM)−3′). Following selection in G418, mClover-positive cells were subcloned by flow sorting. HA-tagged OsTIR1 under the control of a dox-responsive promoter was introduced into WDR70-mAID-mClover cells using lentiviral integration followed by selection in blasticidin and single cell cloning (these cells are hereafter referred to as WDR70-degron cells). Two clones with inducible HA-TIR1 were grown in the presence or absence of IAA and dox for 24 h and harvested for immunoblot. Efficient degradation of WDR70-mAID-mClover was seen in both clones.

Human *DDB1* was targeted for bulk CRISPR KO using the following sgRNAs in the lentiCRISPR v2 plasmid. DDB1 sgRNA # 1: (5′-GGATAGCCATCTGAATTGAG-(PAM)−3′); DDB1 sgRNA # 4: (5′-GCGGCACGTAAAAACCTATG-(PAM)−3′).

4.3. Cell cycle analysis by flow cytometry

Cells were pulsed with 10 μM BrdU for 30 min prior to harvest by trypsinization and fixation in cold 70% ethanol. Cells were washed with 1% BCS in PBS twice, denatured in 2 N HCl for 20 m at room temperature, neutralized in sodium tetraborate, washed again, permeabilized in 0.5% Triton X-100, and washed again. Cells were then labelled with BrdU-FITC conjugated ab (BD, 347583), washed, and then DAPI (0.01 mg/ml) and RNAse A (100 μg/ml) was added prior to analysis on a BD-LSRII system. Standard gating schemes were performed to analyze singlets for BrdU-FITC and DAPI content.

4.4. Immunoblotting

Immunoblotting was performed as described [17] with the following antibodies:

Antibodies		
Gene	**Company**	**Catalog**
53BP1	Abcam	ab175933
53BP1	NovusBio	NB100–304
ARTEMIS	Cell Signaling Technologies	13381
ASTE1	NovusBio	NBP1–8166 1
ATM	NovusBio	nb100–104
BARD1	Santa Cruz	sc11438
BLM	Abcam	ab2179
BRCA1	RD	mab22101
BRCA2	Cell Signaling Technologies	10741
BRCA2	Millipore	OP95
CCDC98	Abcam	ab139191
CTC1	de Lange Lab	
CUL4A	Cell Signaling Technologies	2699
DDB1	Abcam	ab109027
DNAPKcs	Cell Signaling Technologies	38168
EXO1	Abcam	ab95068
γ-Tubulin	Abcam	ab1136
GAPDH	Thermo Fisher	MA5–15738
GFP	Sigma	11814460001
γH2AX	Bethyl	A300–081A
γH2AX	Millipore	05–636
HA	Cell Signaling Technologies	3724

(continued on next page)

(*continued*)

Antibodies		
Gene	**Company**	**Catalog**
Histone 2B	Abcam	ab1790
Histone 2B Ub K120	Cell Signaling Technologies	5546 T
HSP70	BD Biosciences	610608
KU70	Cell Signaling Technologies	4588
KU80	Cell Signaling Technologies	2180
LIG3	BD Biosciences	611876
LIG4	Cell Signaling Technologies	14649
MCM7	Santa Cruz	sc9966
PALB2	Cell Signaling Technologies	30253
PARP1	Enzo	BML-SA249–0050
PCNA	Santa Cruz	sc7907
POLA1	Abcam	65009
POLA2	Abcam	103591
POLR2A	NovusBio	NB200–598
PRIM1	ProteinTech	10773–1
RAD51	Bioacademia	70–001
RAD52	Santa Cruz	365341
RAP80	Bethyl	A300–764A
REV7	Abcam	ab180579
REV7	BD Biosciences	612266
RIF1	de Lange Lab	Silverman et al., 2004 (#1060)
RNF20	Abcam	ab32629
RNF8	Abcam	ab105362
SCC3	Abcam	ab4457
SHLD2	NovusBio	NBP1–88980
SMC1	Abcam	ab9262
STN1	Santa Cruz	sc-376450
STN1	Abcam	89250
WDR70	Santa Cruz	sc-398268
WDR70	Bethyl	A-301–871A
WRN	Abcam	ab124673
XLF	Cell Signaling Technologies	2854
XRCC1	Abcam	ab134056

Band intensity was quantified using FIJI. Band intensity was normalized to loading controls in the linear range after background subtraction.

4.5. Immunofluorescence

Previously published procedures were followed for IF [17] using γH2AX (Millipore), 53BP1 (BD), RIF1, BRCA1, BARD1, RAD51 antibodies. Secondaries used were anti-mouse highly cross-absorbed alexa fluor plus 488 and anti-rabbit highly cross-absorbed alexa fluor plus 647 (Thermo Fisher). Imaging was performed on a DeltaVision (Applied Precision) equipped with a cooled charge-coupled device camera (DV Elite CMOS Camera), a PlanApo 60 × 1.42 NA objective (Olympus America, Inc.), and SoftWoRx software. Deconvoluted images were max projected before scoring foci manually or with automated foci counting software (FIJI). For 53BP1 cavity scoring, samples were blinded from the investigators, and foci were determined to be either cavity-containing, globular, or ambiguous. After excluding ambiguous foci, the percent of foci containing a cavity was derived from the total foci scored.

4.6. Survival assays

WDR70-degron cells were treated with vehicle controls or dox/auxin for 72 h prior to seeding in 6-well plates in duplicate in fresh media without dox/aux. After 8 days, colonies were fixed and stained with 50% methanol, 2% methylene blue, rinsed with water, and dried before counting. The survival percentage compared to untreated cells was calculated.

4.7. RNA extraction, RT-PCR, RNA sequencing

Total RNA was extracted using RNeasy Plus Mini kit (QIAGEN, 74136). cDNA libraries were generated using Trio RNA-Seq kit (Tecan, 0506). For RT-PCR, cDNA was generated using SuperScript IV First-Strand Synthesis System (Thermo Fisher, 18091050). RT-PCR was performed in technical triplicate using SYBR Green PCR Master mix (Applied Biosystems, 4309155) and 0.25 μM concentration of each primer on a QuantStudio 12 K-flex machine (Life Technologies). Fold change with respect to GAPDH was calculated using the ddCt method. A linear range was confirmed for each primer pair by a five-fold serial dilution curve. Primer sequences are listed below. For RNA sequencing, 75 bp paired-end reads were generated by Illumina NextSeq 500.

Gene	Primer Pair	Direction	Sequence (5′−3′)
BRCA1	1	FW	TCATCCAAAGTATGGGCTACAG
BRCA1	1	RV	CTCACAGTTCCAAGGTTAGAGAG
BRCA1	2	FW	CTTCTACAGAGTGAACCCGAAA
BRCA1	2	RV	GTCCTCAGAGTTCTCACAGTTC
BRCA2	1	FW	CAGTGGTATGTGGGAGTTTGT
BRCA2	1	RV	ACCTCAGCTCCTAGACTTTCA
BRCA2	2	FW	AGTTTGTGAAGGGTCGTCAG
BRCA2	2	RV	ACTAAGGGTGGGTGGTGTA
RAD51	1	FW	GGTGAAGGAAAGGCCATGTA
RAD51	1	RV	TCACTGCCAGAGAGACCATA
RAD51	2	FW	GGCAGTGATGTCCTGGATAATG
RAD51	2	RV	CCATCATGGCTGATGCTTGATA
BARD1	1	FW	GGCGACATACCTTCTGTTGA
BARD1	1	RV	CCTTCAGGTGCCCATGATT
BARD1	2	FW	CATGAAGCTTGCAATCATGGG
BARD1	2	RV	TCGTGAAGTGGTGAGTCATTT
53BP1	1	FW	GAGGAAGGTGGGTGTTCTTT
53BP1	1	RV	CAGGAGAAGGAGCAACAAGAT
53BP1	2	FW	CCCTTGTTCAGGACAGTCTTT
53BP1	2	RV	TGGGACTGCTAGGAACGATA
STN1	1	FW	CACATACAGAGAAGAGCGAGAG
STN1	1	RV	GTAGATAGTGGGCAGCTCAAG
STN1	2	FW	CAGTATCCGCACATACAGAGAAG
STN1	2	RV	GCTCAAGCATCCTTGCAATTT
REV7	1	FW	GAGAAGATCCAGGTCATCAAGG
REV7	1	RV	ATGTCCGACGTCATGGTTT
REV7	2	FW	CACTCGCAACATGGAGAAGA
REV7	2	RV	CATGTGGACATCCTGCTCAT
GAPDH	1	FW	GGTGTGAACCATGAGAAGTATGA
GAPDH	1	RV	GAGTCCTTCCACGATACCAAAG
GAPDH	2	FW	ATGTTCGTCATGGGTGTGAA
GAPDH	2	RV	ACGATACCAAAGTTGTCATGGA

4.8. RNAseq processing and analysis

Sequence and transcript coordinates for human hg38 UCSC genome and gene models were retrieved from the Bioconductor Bsgenome. Hsapiens.UCSC.hg38 (version 1.4.0) and TxDb.Hsapiens.UCSC.hg38. knownGene (version 3.4.0) Bioconductor libraries respectively. Transcript expressions were calculated using the Salmon quantification software [53] (version 0.8.2) and gene expression levels as TPMs and counts retrieved using Tximport [54] (version 1.8.0). Normalization and rlog transformation of raw read counts in genes were performed using DESeq2 [54] (version 1.20.0). For visualization in genome browsers, RNA-seq reads are aligned to the genome using Rsubread's subjunc method (version 1.30.6) [55] and exported as bigWigs normalised to reads per million using the rtracklayer package (version 1.40.6). Genes were identified as differentially expressed between conditions using DESeq2 with a Benjamini Hochberg adjusted p-value cutoff of 0.05. Gene sets were retrieved from MsigDB c2 pathway gene sets (version 7.0), and gene set enrichment analysis was performed using the R Bioconductor fgsea package [56]. For visualization of gene sets, single sample GSEA analysis was performed using GSVA (version 1.34.0) [57] and heat maps were drawn using the pheatmap R package.

4.9. Statistical analysis

Details pertaining to all statistical testing (including N and P values) can be found in the appropriate figure legends.

CRediT authorship contribution statement

Zachary Mirman: Conceptualization, Methodology, Investigation, Writing – original draft, Writing – review & editing. **Keshav Sharma:** Methodology, Investigation. **Thomas S. Carroll:** Formal analysis. **Titia de Lange:** Conceptualization, Writing – original draft, Writing – review & editing.

Funding

National Cancer Institute F99 award 1F99CA245720–01 (ZM). National Cancer Institute 5 R35 CA210036 (TdL). Breast Cancer Research Foundation BCRF-19–036 (TdL). Melanoma Research Alliance MRA#577521 (TdL). TdL is an American Cancer Society Rose Zarucki Trust Research Professor.

Declaration of Competing Interest

For the manuscript: **"Expression of BRCA1, BRCA2, RAD51, and other DSB repair factors is regulated by CRL4^{WDR70}"**:

TdL is a member of the Scientific Advisory Board of Calico Life Sciences. The remaining authors declare no conflicts of interest.

Data and materials availability

Data supporting the findings of this study are available within the article and its supplementary data. RNAseq data has been deposited in GEO (Bioproject ID PRJNA784996) and was validated using quantitative PCR.

Acknowledgments

We thank Zhe Yang for generating p53/RB-null RPE1 cells, and Nanda Sasi for help designing auxin-induced degron reagents. Leonid Timashev and Zhe Yang are thanked for developing FIJI image analysis macros. Roger Greenberg is thanked for sharing U2OS-FOKI-LacI cells, and we thank Dan Durocher for *BRCA1/SHLD2* KO RPE1 cells. Nathaniel Heintz, Christina Pressl, Kert Matlik, Cuidong Wang, and Connie Zhao (Genomics Resource Center) are thanked for assistance with RNA sample preparation and sequencing.

Appendix A. Supporting information

Supplementary data associated with this article can be found in the online version at doi:10.1016/j.dnarep.2022.103320.

References

[1] A. Ciccia, S.J. Elledge, The DNA damage response: making it safe to play with knives, Mol. Cell 40 (2010) 179.
[2] N. Hustedt, D. Durocher, The control of DNA repair by the cell cycle, Nat. Cell Biol. 19 (2016) 1.
[3] W.D. Wright, S.S. Shah, W.D. Heyer, Homologous recombination and the repair of DNA double-strand breaks, J. Biol. Chem. 293 (2018) 10524.
[4] R. Roy, J. Chun, S.N. Powell, BRCA1 and BRCA2: different roles in a common pathway of genome protection, Nat. Rev. Cancer 12 (2011) 68.
[5] W. Zhao, J.B. Steinfeld, F. Liang, X. Chen, D.G. Maranon, C. Jian Ma, Y. Kwon, T. Rao, W. Wang, C. Sheng, X. Song, Y. Deng, J. Jimenez-Sainz, L. Lu, R.B. Jensen, Y. Xiong, G.M. Kupfer, C. Wiese, E.C. Greene, P. Sung, BRCA1-BARD1 promotes RAD51-mediated homologous DNA pairing, Nature 550 (2017) 360.
[6] H. Farmer, N. McCabe, C.J. Lord, A.N. Tutt, D.A. Johnson, T.B. Richardson, M. Santarosa, K.J. Dillon, I. Hickson, C. Knights, N.M. Martin, S.P. Jackson, G. C. Smith, A. Ashworth, Targeting the DNA repair defect in BRCA mutant cells as a therapeutic strategy, Nature 434 (2005) 917.
[7] S.F. Bunting, E. Callén, N. Wong, H.T. Chen, F. Polato, A. Gunn, A. Bothmer, N. Feldhahn, O. Fernandez-Capetillo, L. Cao, X. Xu, C.X. Deng, T. Finkel, M. Nussenzweig, J.M. Stark, A. Nussenzweig, 53BP1 inhibits homologous recombination in Brca1-deficient cells by blocking resection of DNA breaks, Cell 141 (2010) 243.
[8] P. Bouwman, A. Aly, J.M. Escandell, M. Pieterse, J. Bartkova, H. van der Gulden, S. Hiddingh, M. Thanasoula, A. Kulkarni, Q. Yang, B.G. Haffty, J. Tommiska, C. Blomqvist, R. Drapkin, D.J. Adams, H. Nevanlinna, J. Bartek, M. Tarsounas, S. Ganesan, J. Jonkers, 53BP1 loss rescues BRCA1 deficiency and is associated with triple-negative and BRCA-mutated breast cancers, Nat. Struct. Mol. Biol. 17 (2010) 688.
[9] M. Zimmermann, F. Lottersberger, S.B. Buonomo, A. Sfeir, T. de Lange, 53BP1 regulates DSB repair using Rif1 to control 5′ end resection, Science 339 (2013) 700.
[10] C. Escribano-Díaz, A. Orthwein, A. Fradet-Turcotte, M. Xing, J.T. Young, J. Tkáč, M.A. Cook, A.P. Rosebrock, M. Munro, M.D. Canny, D. Xu, D. Durocher, A cell cycle-dependent regulatory circuit composed of 53BP1-RIF1 and BRCA1-CtIP controls DNA repair pathway choice, Mol. Cell 49 (2013) 872.
[11] L. Feng, K.W. Fong, J. Wang, W. Wang, J. Chen, RIF1 counteracts BRCA1-mediated end resection during DNA repair, J. Biol. Chem. 288 (2013) 11135.
[12] J.R. Chapman, P. Barral, J.B. Vannier, V. Borel, M. Steger, A. Tomas-Loba, A. A. Sartori, I.R. Adams, F.D. Batista, S.J. Boulton, RIF1 is essential for 53BP1-dependent nonhomologous end joining and suppression of DNA double-strand break resection, Mol. Cell 49 (2013) 858.
[13] M. Di Virgilio, E. Callen, A. Yamane, W. Zhang, M. Jankovic, A.D. Gitlin, N. Feldhahn, W. Resch, T.Y. Oliveira, B.T. Chait, A. Nussenzweig, R. Casellas, D. F. Robbiani, M.C. Nussenzweig, Rif1 prevents resection of DNA breaks and promotes immunoglobulin class switching, Science 339 (2013) 711.
[14] V. Boersma, N. Moatti, S. Segura-Bayona, M.H. Peuscher, J. van der Torre, B. A. Wevers, A. Orthwein, D. Durocher, J.J.L. Jacobs, MAD2L2 controls DNA repair at telomeres and DNA breaks by inhibiting 5′ end resection, Nature 521 (2015) 537.
[15] G. Xu, J.R. Chapman, I. Brandsma, J. Yuan, M. Mistrik, P. Bouwman, J. Bartkova, E. Gogola, D. Warmerdam, M. Barazas, J.E. Jaspers, K. Watanabe, M. Pieterse, A. Kersbergen, W. Sol, P.H.N. Celie, P.C. Schouten, B. van den Broek, A. Salman, M. Nieuwland, I. de Rink, J. de Ronde, K. Jalink, S.J. Boulton, J. Chen, D.C. van Gent, J. Bartek, J. Jonkers, P. Borst, S. Rottenberg, REV7 counteracts DNA double-strand break resection and affects PARP inhibition, Nature 521 (2015) 541.
[16] H. Ghezraoui, C. Oliveira, J.R. Becker, K. Bilham, D. Moralli, C. Anzilotti, R. Fischer, M. Deobagkar-Lele, M. Sanchiz-Calvo, E. Fueyo-Marcos, S. Bonham, B. M. Kessler, S. Rottenberg, R.J. Cornall, C.M. Green, J.R. Chapman, 53BP1 cooperation with the REV7-shieldin complex underpins DNA structure-specific NHEJ, Nature 560 (2018) 122.
[17] Z. Mirman, F. Lottersberger, H. Takai, T. Kibe, Y. Gong, K. Takai, A. Bianchi, M. Zimmermann, D. Durocher, T. de Lange, 53BP1-RIF1-shieldin counteracts DSB resection through CST- and Polα-dependent fill-in, Nature 560 (2018) 112.
[18] R. Gupta, K. Somyajit, T. Narita, E. Maskey, A. Stanlie, M. Kremer, D. Typas, M. Lammers, N. Mailand, A. Nussenzweig, J. Lukas, C. Choudhary, DNA repair network analysis reveals shieldin as a key regulator of NHEJ and PARP inhibitor sensitivity, Cell 173 (2018) 972.
[19] M. Barazas, S. Annunziato, S.J. Pettitt, I. de Krijger, H. Ghezraoui, S.J. Roobol, C. Lutz, J. Frankum, F.F. Song, R. Brough, B. Evers, E. Gogola, J. Bhin, M. van de Ven, D.C. van Gent, J.J.L. Jacobs, R. Chapman, C.J. Lord, J. Jonkers, S. Rottenberg, The CST complex mediates end protection at double-strand breaks and promotes PARP inhibitor sensitivity in BRCA1-deficient cells, Cell Rep. 23 (2018) 2107.
[20] S.M. Noordermeer, S. Adam, D. Setiaputra, M. Barazas, S.J. Pettitt, A.K. Ling, M. Olivieri, A. Álvarez-Quilón, N. Moatti, M. Zimmermann, S. Annunziato, D. B. Krastev, F. Song, I. Brandsma, J. Frankum, R. Brough, A. Sherker, S. Landry, R. K. Szilard, M.M. Munro, A. McEwan, T. Goullet de Rugy, Z.Y. Lin, T. Hart, J. Moffat, A.C. Gingras, A. Martin, H. van Attikum, J. Jonkers, C.J. Lord, S. Rottenberg, D. Durocher, The shieldin complex mediates 53BP1-dependent DNA repair, Nature 560 (2018) 117.
[21] S. Panier, S.J. Boulton, Double-strand break repair: 53BP1 comes into focus, Nat. Rev. Mol. Cell Biol. 15 (2014) 7.
[22] Z. Mirman, T. de Lange, 53BP1: a DSB escort, Genes Dev. 34 (2020) 7.
[23] A. Sfeir, L.S. Symington, Microhomology-mediated end joining: a back-up survival mechanism or dedicated pathway, Trends Biochem Sci. 40 (2015) 701.
[24] H.H.Y. Chang, N.R. Pannunzio, N. Adachi, M.R. Lieber, Non-homologous DNA end joining and alternative pathways to double-strand break repair, Nat. Rev. Mol. Cell Biol. 18 (2017) 495.
[25] M. Zeng, L. Ren, K. Mizuno, K. Nestoras, H. Wang, Z. Tang, L. Guo, D. Kong, Q. Hu, Q. He, L. Du, A.M. Carr, C. Liu, CRL4(Wdr70) regulates H2B monoubiquitination and facilitates Exo1-dependent resection, Nat. Commun. 7 (2016) 11364.
[26] S. Jackson, Y. Xiong, CRL4s: the CUL4-RING E3 ubiquitin ligases, Trends Biochem Sci. 34 (2009) 562.
[27] J.M. Li, J. Jin, CRL ubiquitin ligases and DNA damage response, Front Oncol. 2 (2012) 29.
[28] M. Zeng, Z. Tang, L. Guo, X. Wang, C. Liu, Wdr70 regulates histone modification and genomic maintenance in fission yeast, Biochim Biophys. Acta Mol. Cell Res 1867 (2020), 118665.
[29] L.D. Guo, D. Wang, F. Yang, Y.J. Liang, X.Q. Yang, Y.Y. Qin, L.F. Ren, M. Zeng, Z. Z. Tang, X.J. Wang, S. Wang, C. Liu, J.Y. Lou, J. Chen, [Functional Analysis of DNA Damage Repair Factor WDR70 and Its Mutation in Ovarian Cancer, Sichuan Da Xue Xue Bao Yi Xue Ban. 47 (2016) 501.
[30] C.J. Lord, S. McDonald, S. Swift, N.C. Turner, A. Ashworth, A high-throughput RNA interference screen for DNA repair determinants of PARP inhibitor sensitivity, DNA Repair (Amst.) 7 (2008) 2010.

[31] M. Weber, B. Beyene, N. Nagler, J. Herfert, S. Schempp, M. Klecker, S. Clemens, A mutation in the essential and widely conserved DAMAGED DNA BINDING1-Cullin4 ASSOCIATED FACTOR gene OZS3 causes hypersensitivity to zinc excess, cold and UV stress in Arabidopsis thaliana, Plant J. 103 (2020) 995.
[32] T. Natsume, T. Kiyomitsu, Y. Saga, M.T. Kanemaki, Rapid protein depletion in human cells by auxin-inducible degron tagging with short homology donors, Cell Rep. 15 (2016) 210.
[33] Z. Yang, J. Maciejowski, T. de Lange, Nuclear envelope rupture is enhanced by loss of p53 or Rb, Mol. Cancer Res. 15 (2017) 1579.
[34] D. Setiaputra, D. Durocher, Shieldin - the protector of DNA ends, EMBO Rep. 20 (2019).
[35] F. Zhao, W. Kim, H. Gao, C. Liu, Y. Zhang, Y. Chen, M. Deng, Q. Zhou, J. Huang, Q. Hu, S.H. Chen, S. Nowsheen, J.A. Kloeber, B. Qin, P. Yin, X. Tu, G. Guo, S. Qin, C. Zhang, M. Gao, K. Luo, Y. Liu, Z. Lou, J. Yuan, ASTE1 promotes shieldin-complex-mediated DNA repair by attenuating end resection, Nat. Cell Biol. 23 (2021) 894.
[36] J.R. Chapman, A.J. Sossick, S.J. Boulton, S.P. Jackson, BRCA1-associated exclusion of 53BP1 from DNA damage sites underlies temporal control of DNA repair, J. Cell Sci. 125 (2012) 3529.
[37] F. Ochs, G. Karemore, E. Miron, J. Brown, H. Sedlackova, M.B. Rask, M. Lampe, V. Buckle, L. Schermelleh, J. Lukas, C. Lukas, Stabilization of chromatin topology safeguards genome integrity, Nature 574 (2019) 571.
[38] Y.J. He, C.M. McCall, J. Hu, Y. Zeng, Y. Xiong, DDB1 functions as a linker to recruit receptor WD40 proteins to CUL4-ROC1 ubiquitin ligases, Genes Dev. 20 (2006) 2949.
[39] T.A. Soucy, P.G. Smith, M.A. Milhollen, A.J. Berger, J.M. Gavin, S. Adhikari, J. E. Brownell, K.E. Burke, D.P. Cardin, S. Critchley, C.A. Cullis, A. Doucette, J. J. Garnsey, J.L. Gaulin, R.E. Gershman, A.R. Lublinsky, A. McDonald, H. Mizutani, U. Narayanan, E.J. Olhava, S. Peluso, M. Rezaei, M.D. Sintchak, T. Talreja, M. P. Thomas, T. Traore, S. Vyskocil, G.S. Weatherhead, J. Yu, J. Zhang, L.R. Dick, C. F. Claiborne, M. Rolfe, J.B. Bolen, S.P. Langston, An inhibitor of NEDD8-activating enzyme as a new approach to treat cancer, Nature 458 (2009) 732.
[40] L. Litovchick, S. Sadasivam, L. Florens, X. Zhu, S.K. Swanson, S. Velmurugan, R. Chen, M.P. Washburn, X.S. Liu, J.A. DeCaprio, Evolutionarily conserved multisubunit RBL2/p130 and E2F4 protein complex represses human cell cycle-dependent genes in quiescence, Mol. Cell 26 (2007) 539.
[41] K. Engeland, Cell cycle arrest through indirect transcriptional repression by p53: I have a DREAM, Cell Death Differ. 25 (2018) 114.
[42] M. Fischer, L. Steiner, K. Engeland, The transcription factor p53: not a repressor, solely an activator, Cell Cycle 13 (2014) 3037.
[43] M. Fischer, P. Grossmann, M. Padi, J.A. DeCaprio, Integration of TP53, DREAM, MMB-FOXM1 and RB-E2F target gene analyses identifies cell cycle gene regulatory networks, Nucleic Acids Res. 44 (2016) 6070.
[44] K. Nakamura, A. Kato, J. Kobayashi, H. Yanagihara, S. Sakamoto, D.V. Oliveira, M. Shimada, H. Tauchi, H. Suzuki, S. Tashiro, L. Zou, K. Komatsu, Regulation of homologous recombination by RNF20-dependent H2B ubiquitination, Mol. Cell 41 (2011) 515.
[45] L. Moyal, Y. Lerenthal, M. Gana-Weisz, G. Mass, S. So, S.Y. Wang, B. Eppink, Y. M. Chung, G. Shalev, E. Shema, D. Shkedy, N.I. Smorodinsky, N. van Vliet, B. Kuster, M. Mann, A. Ciechanover, J. Dahm-Daphi, R. Kanaar, M.C. Hu, D. J. Chen, M. Oren, Y. Shiloh, Requirement of ATM-dependent monoubiquitylation of histone H2B for timely repair of DNA double-strand breaks, Mol. Cell 41 (2011) 529.
[46] L. Ren, M. Zeng, Z. Tang, M. Li, X. Wang, Y. Xu, Y. Weng, X. Wang, H. Wang, L. Guo, B. Zuo, X. Wang, S. Wang, J. Lou, Y. Tang, D. Mu, N. Zheng, X. Wu, J. Han, A.M. Carr, P. Jeggo, C. Liu, The antiresection activity of the X protein encoded by hepatitis virus B, Hepatology 69 (2019) 2546.
[47] B.R. Chen, Y. Wang, A. Tubbs, D. Zong, F.C. Fowler, N. Zolnerowich, W. Wu, A. Bennett, C.C. Chen, W. Feng, A. Nussenzweig, J.K. Tyler, B.P. Sleckman, LIN37-DREAM prevents DNA end resection and homologous recombination at DNA double-strand breaks in quiescent cells, Elife 10 (2021), e68466.
[48] K. Somyajit, J. Spies, F. Coscia, U. Kirik, M.B. Rask, J.H. Lee, K.J. Neelsen, A. Mund, L.J. Jensen, T.T. Paull, M. Mann, J. Lukas, Homology-directed repair protects the replicating genome from metabolic assaults, Dev. Cell 56 (2021) 461.
[49] R.S. Bindra, P.J. Schaffer, A. Meng, J. Woo, K. Måseide, M.E. Roth, P. Lizardi, D. W. Hedley, R.G. Bristow, P.M. Glazer, Down-regulation of Rad51 and decreased homologous recombination in hypoxic cancer cells, Mol. Cell Biol. 24 (2004) 8504.
[50] N. Chan, M. Koritzinsky, H. Zhao, R. Bindra, P.M. Glazer, S. Powell, A. Belmaaza, B. Wouters, R.G. Bristow, Chronic hypoxia decreases synthesis of homologous recombination proteins to offset chemoresistance and radioresistance, Cancer Res 68 (2008) 605.
[51] K. Bertram, L. El Ayoubi, O. Dybkov, D.E. Agafonov, C.L. Will, K. Hartmuth, H. Urlaub, B. Kastner, H. Stark, R. Lührmann, Structural Insights into the roles of metazoan-specific splicing factors in the human step 1 spliceosome, Mol. Cell 80 (2020) 127.
[52] P. Wu, H. Takai, T. de Lange, Telomeric 3′ overhangs derive from resection by Exo1 and Apollo and fill-in by POT1b-associated CST, Cell 150 (2012) 39.
[53] R. Patro, G. Duggal, M.I. Love, R.A. Irizarry, C. Kingsford, Salmon provides fast and bias-aware quantification of transcript expression, Nat. Methods 14 (2017) 417.
[54] M.I. Love, C. Soneson, R. Patro, Swimming downstream: statistical analysis of differential transcript usage following Salmon quantification, F1000Res. 7 (2018) 952.
[55] Y. Liao, G.K. Smyth, W. Shi, The Subread aligner: fast, accurate and scalable read mapping by seed-and-vote, Nucleic Acids Res 41 (2013), e108.
[56] A. Subramanian, P. Tamayo, V.K. Mootha, S. Mukherjee, B.L. Ebert, M.A. Gillette, A. Paulovich, S.L. Pomeroy, T.R. Golub, E.S. Lander, J.P. Mesirov, Gene set enrichment analysis: a knowledge-based approach for interpreting genome-wide expression profiles, Proc. Natl. Acad. Sci. USA 102 (2005) 15545.
[57] S. Hänzelmann, R. Castelo, J. Guinney, GSVA: gene set variation analysis for microarray and RNA-seq data, BMC Bioinforma. 14 (2013) 7.
[58] Z. Mirman, N. Kumar Sasi, A. King, J. Ross Chapman, T. de Lange, 53BP1-shieldin-dependent DSB processing in BRCA1-deficient cells requires CST-Polα-primase fill-in synthesis, Nat. Cell Biol. 24 (1) (2022) 51–61, https://doi.org/10.1038/s41556-021-00812-9.

Supplementary Materials for

Expression of BRCA1, BRCA2, RAD51, and other DSB repair factors is regulated by $CRL4^{WDR70}$

Zachary Mirman, Keshav Sharma, Thomas S. Carroll, and Titia de Lange*

* To whom correspondence should be addressed: Titia de Lange delange@rockefeller.edu

Mirman et al. Fig. S1

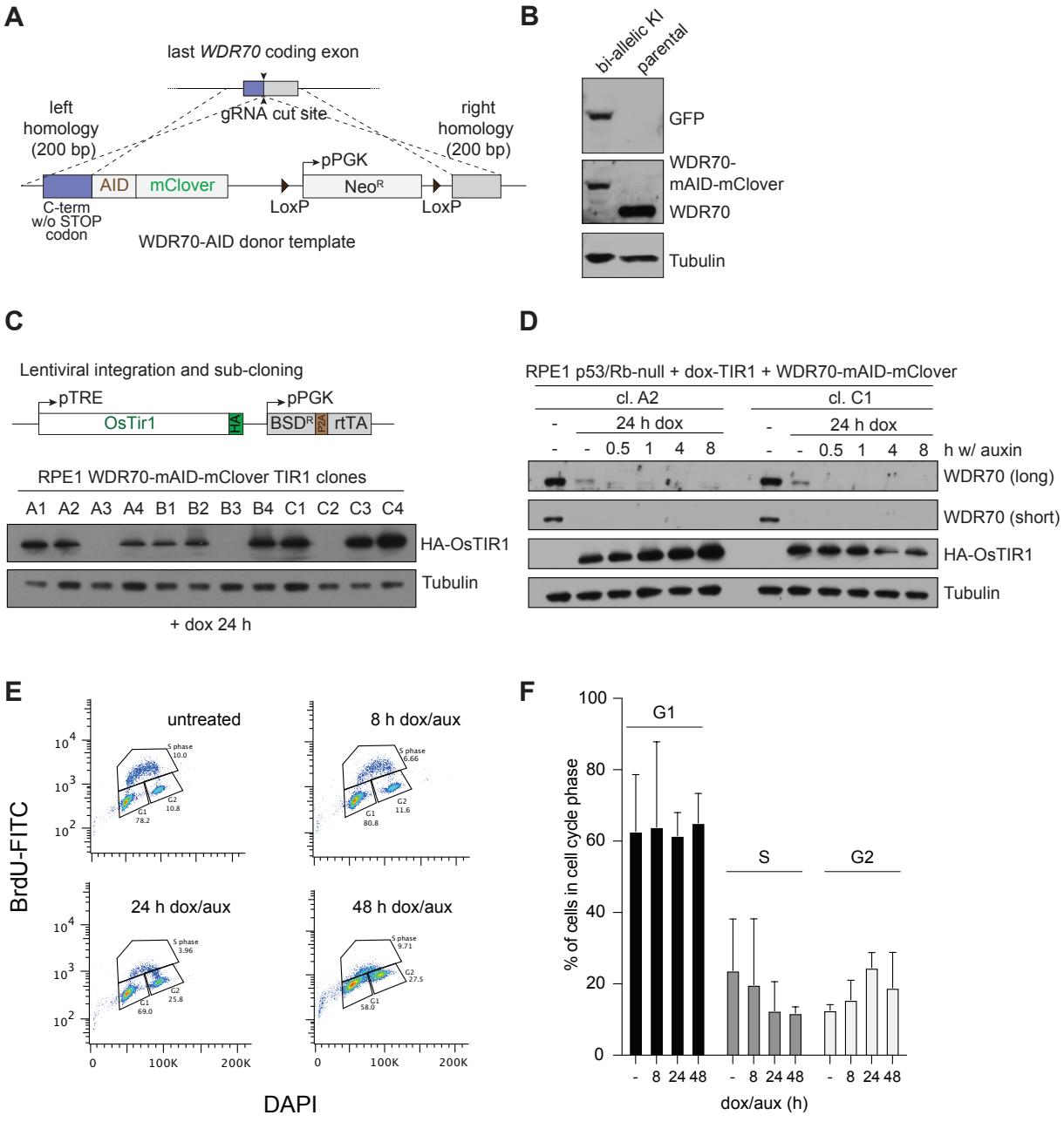

Fig. S1. Generation of RPE1 cells for rapid WDR70 degradation. (A) Schematic representation of insertion of mAID-mClover cassette into both *WDR70* alleles of p53/RB-null RPE1 cells. **(B)** Immunoblot for GFP and WDR70 showing a representative biallelic knock-in (KI) WDR70-degron candidate and the parental cell line for comparison. **(C)** Immunoblot for HA-tagged OsTIR1 after doxycycline induction in 12 candidate subclones. Clones A2 and C1 were selected for further study. **(D)** Immunoblots showing dox/auxin-mediated degradation of WDR70 in two clones. Clone A2 was used for the remainder of the study, and this blot (cropped) is reproduced in Figure 1**B**. **(E)** Cell cycle flow cytometry plots for BrdU incorporation (30 m pulse of BrdU before fixation) and DAPI content in WDR70-degron cells with dox/auxin treatment for the indicated time. **(F)** Quantification of cell cycle phase as represented in (**E**). Data from three independent experiments.

Mirman et al. Fig. S2

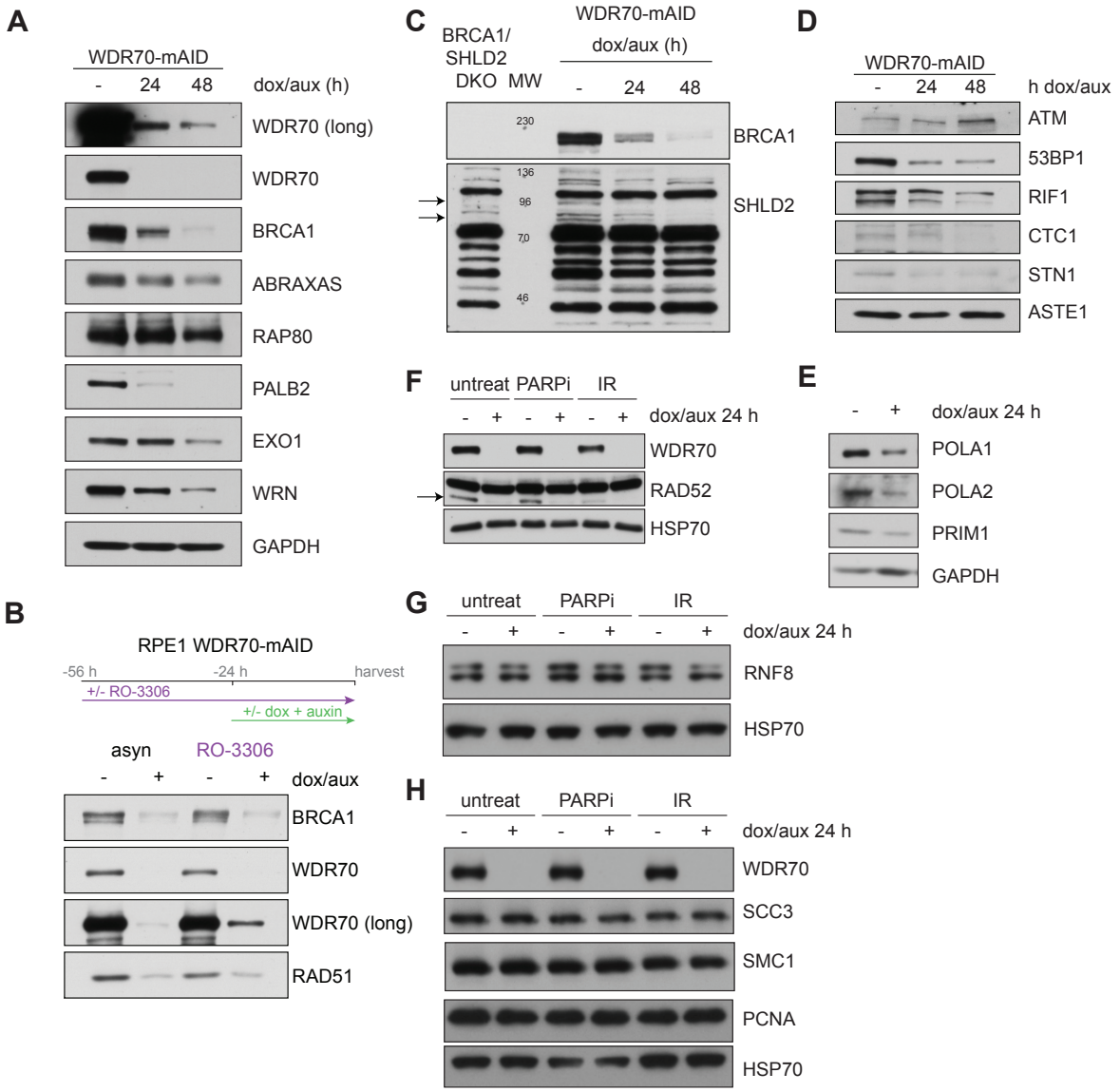

Fig. S2. WDR70 loss leads to reduced protein levels for HDR and 53BP1 pathway components. (**A**) Immunoblots for BRCA-associated targets in WDR70-degron cells after 24 or 48 hr dox/aux treatment. (**B**) Immunoblots for the indicated proteins in WDR70-degron cells with or without the CDK1 inhibitor RO-3306 according to the experimental timeline shown. (**C**) *BRCA1/SHLD2* DKO RPE1 cells (20) were used to validate the SHLD2 antibody which has many non-specific bands. Arrows indicate two bands that are absent in the *BRCA1/SHLD2* DKO but present in WDR70-degron cells. These bands decrease after 24 or 48 hr dox/aux treatment. (**D**) Immunoblots as in **(A)** for the indicated proteins from the 53BP1 pathway. (**E**) Immunoblots for the indicated proteins from the Polα/primase complex in WDR70-degron cells with or without dox/aux treatment for 24 h. **(F)** Immunoblot for RAD52 in WDR70-degron cells with the indicated treatments. **(G)** Immunoblot for RNF8 in cells as in **(F)**. **(H)** Immunoblot for the indicated proteins in cells as in **(F)**. All blots representative of two or more independent experiments. GAPDH or HSP70 are used as loading controls and are unaffected by WDR70 loss. Protein concentrations were also checked by BCA assay and Ponceau stains to ensure equal loading.

Mirman et al. Fig. S3

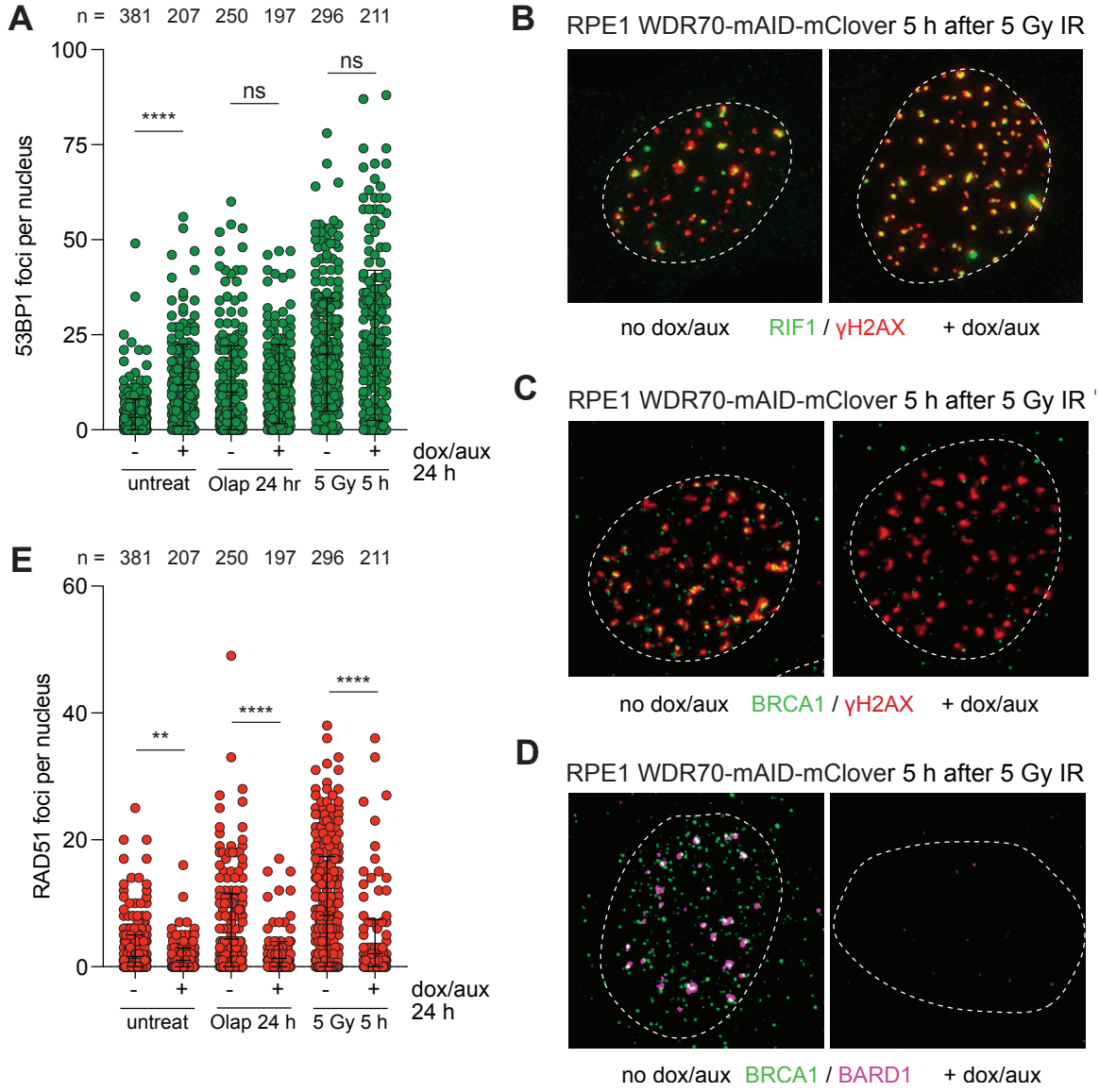

Fig. S3. The effect of WDR70 loss on DNA damage foci. (A) Automated foci scoring of 53BP1 foci per nucleus in WDR70-degron cells with the indicated treatments. The number of nuclei (n) pooled from three independent experiments is indicated. **(B)** Representative IF images of RIF1 (green) and γH2AX (red) in irradiated cells with or without 24 h dox/auxin treatment. **(C)** Representative IF images of BRCA1 (green) and γH2AX (red) in cells as in **(B)**. **(D)** Representative IF images of BRCA1 (green) and BARD1 (magenta) in cells as in **(B). (E)** Automated foci scoring of RAD51 foci per nucleus in WDR70-degron cells with the indicated treatments. The number of nuclei (n) pooled from three independent experiments is indicated. Dashed lines demarcate nuclear outlines. All panels representative of three independent experiments. Statistical analyses as in Figure 1.

Mirman et al. Fig. S4

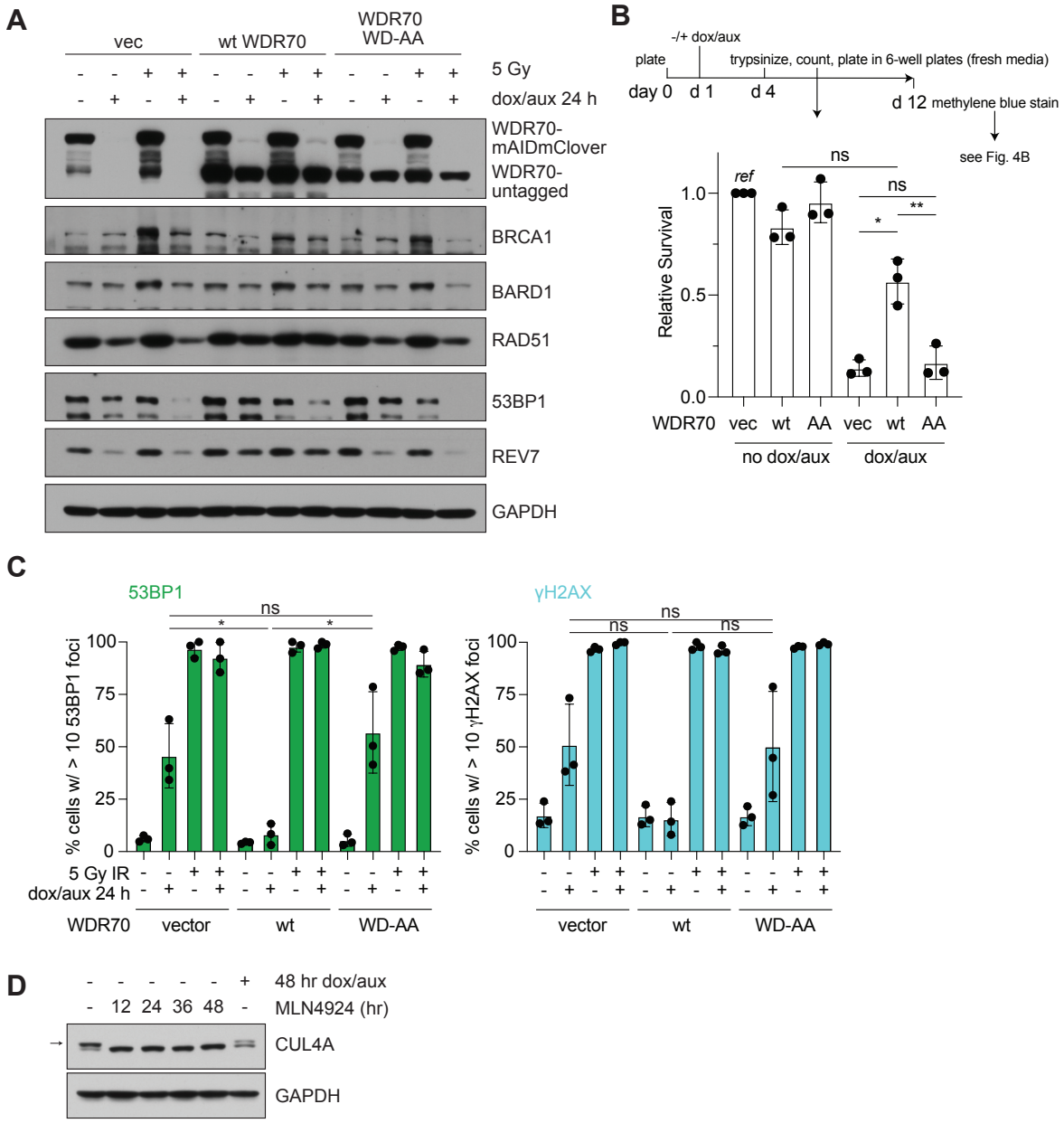

Fig. S4. WDR70 functions via its DWD motif as part of a CRL4 complex. (A) Immunoblots for the indicated proteins in WDR70-degron cells complemented with empty vector (vec) or the indicated WDR70 constructs. Cells were treated with IR (5 h after 5 Gy) and/or dox/auxin for 24 h as indicated. In the top blot, WDR70 antibody detects the knock-in mAID-mClover-tagged WDR70 and the exogenously-expressed untagged WDR70 wild-type or WD-AA mutant. **(B)** Experimental schematic of cell survival assay for WDR70-degron cells complemented with empty vector or the indicated WDR70 constructs. Bottom, relative survival of the indicated cells after 72 h of dox/aux treatment, normalized to empty vector cells with no dox/aux. Survival is normalized to vector-containing cells with no dox/aux (ref). **(C)** Quantification of percent of cells with greater than 10 foci in cells as in **(A)**. Bar graph depicts mean and sd from three independent experiments. **(D)** Immunoblot for CUL4A after treatment with MLN4924, resulting in the disappearance of the top band (arrow), which likely represents NEDD8-conjugated CUL4A. Statistical analyses as in Figure 1.

Mirman et al. Fig. S5

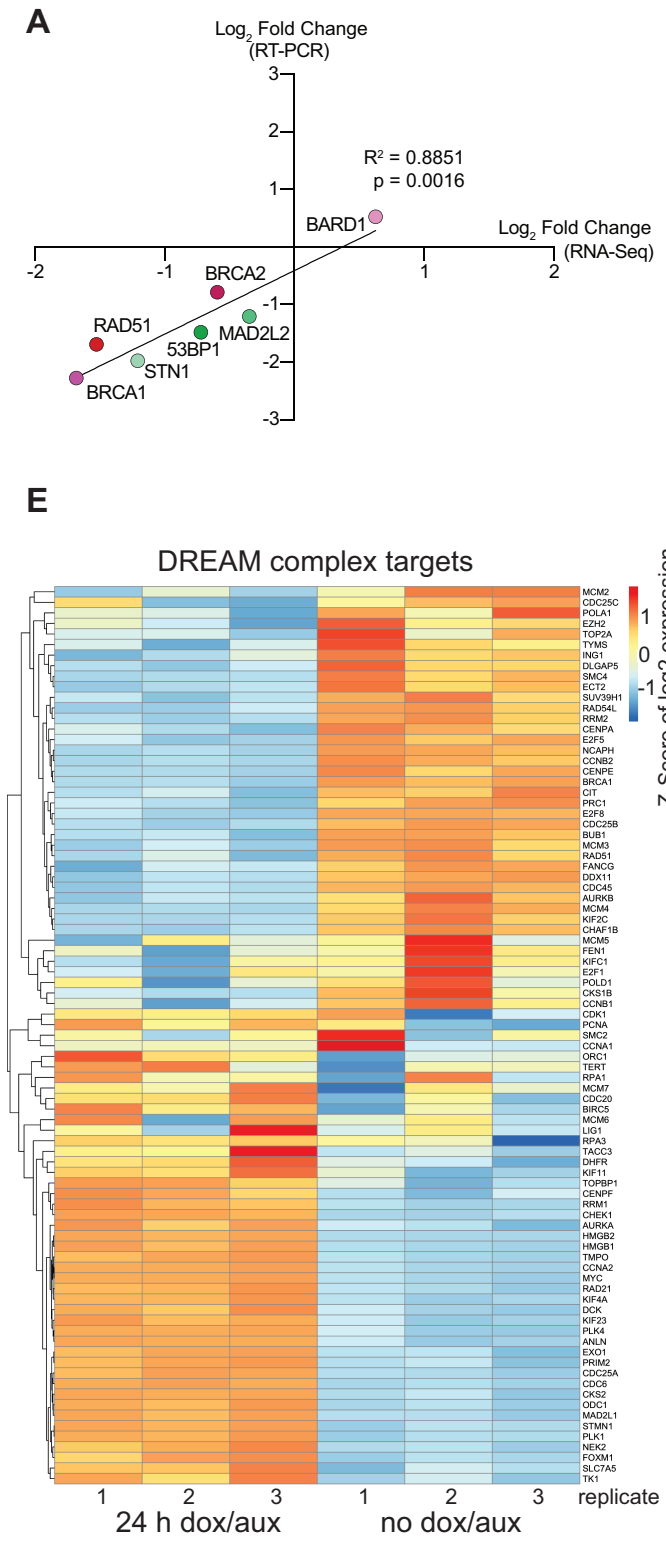

71
72

Fig. S5. WDR70 loss affects RNA levels of DDR and other factors. (A) Correlation between Log_2 fold change derived from RT-PCR (y-axis) and Log_2 fold change derived from RNAseq (x-axis) for the indicated genes. Simple linear regression was performed to determine the R^2 value, and the p value indicates a slope which is significantly non-zero. **(B)** Quantification of band intensity after WDR70 degradation from western blots in Fig. 2, Fig. S2 and independent biological replicates. Reference line at 1.0 (ref) is protein level without addition of dox and aux. One-way ANOVA analysis with Dunnett's correction for multiple hypothesis testing was performed. **(C, D)** Volcano plot depicting Log_2 fold change and absolute Wald Statistic for transcripts in WDR70-depleted cells (dox and aux 24 h). Negative Log_2 fold change (blue dots and labels) indicates transcripts which are less abundant in WDR70-depleted cells. Positive Log_2 fold change (red dots and labels) indicates transcripts which are more abundant in WDR70-depleted cells. Absolute Wald Statistic above 1.96 (marked by the dashed line) is considered significant. Black dots and labels indicate genes which were not differentially regulated. **(C)** Transcripts of factors involved in repair by classical non-homologous end-joining are highlighted. **(D)** Transcripts of factors involved in repair by alternative non-homologous end-joining are highlighted. **(E)** Differential expression analysis of putative DREAM targets in Fig. 5E. **(F)** RNAseq and immunoblot analysis of POLR2A. Top, average normalized POLR2A counts from three technical replicates in dox/aux-treated and control WDR70-degron cells (Log_2 fold change = -1.90; $p = 1.37 \times 10^{-8}$). Bottom, immunoblot showing POLR2A levels in the same cells. Representative of two independent experiments. Statistical analyses as in Figure 1 except where otherwise indicated.

Mirman et al. Fig. S6

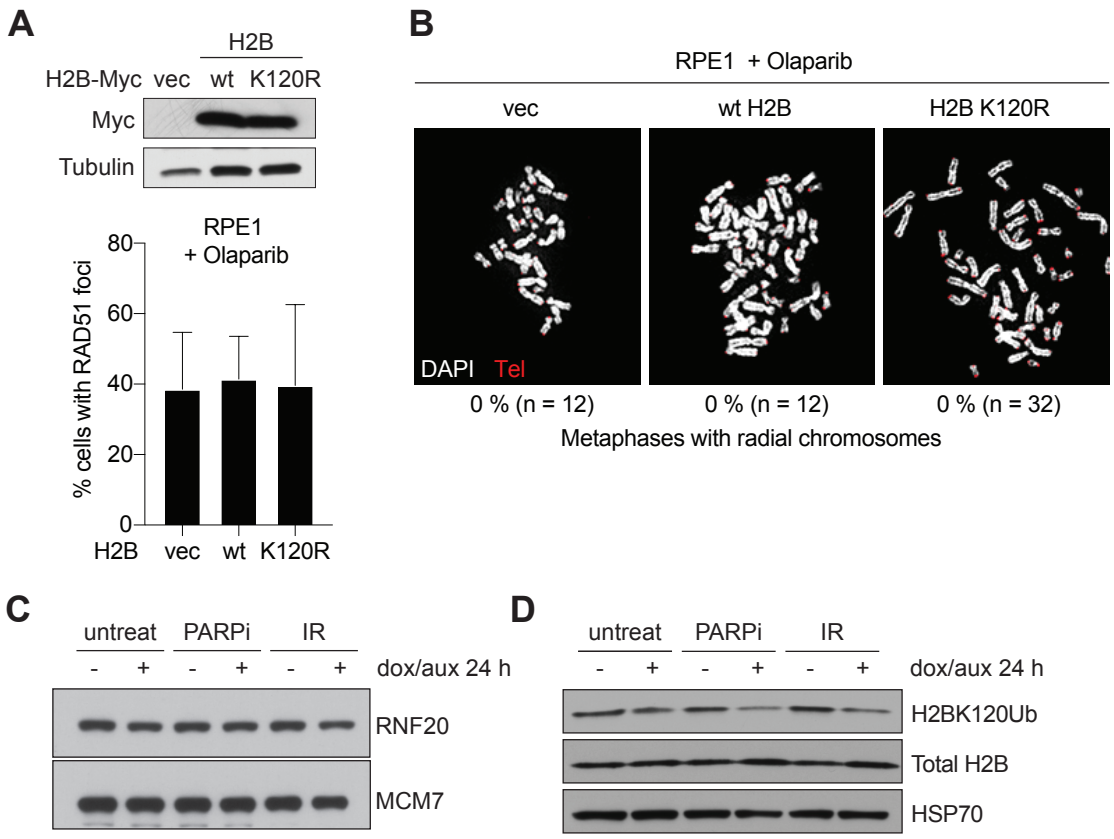

Fig. S6. H2BK120R does not affect RAD51 loading or PARPi-induced radial formation. (**A**) Top, Immunoblot showing expression of transfected empty vector (vec), wild-type (wt) or dominant negative (K120R) H2B constructs in RPE1 cells. Bottom, PARPi-induced RAD51 foci formation in cells as in **(A)**. **(B)** Analysis of PARPi-treated DAPI-stained metaphase spreads from cells as in **(A)**. **(C)** Immunoblot for RNF20 after WDR70 degradation in WDR70-degron cells with the indicated treatments. MCM7 is used as a loading control. **(D)** Immunoblot for H2BK120Ub after WDR70 degradation in cells as in **(C)**. All panels representative of two independent experiments. Protein amounts were ensured to be even by BCA assay and ponceau stain.